iScience

CellPress
OPEN ACCESS

Article

A desmosomal cadherin controls multipotent hair follicle stem cell quiescence and orchestrates regeneration through adhesion signaling

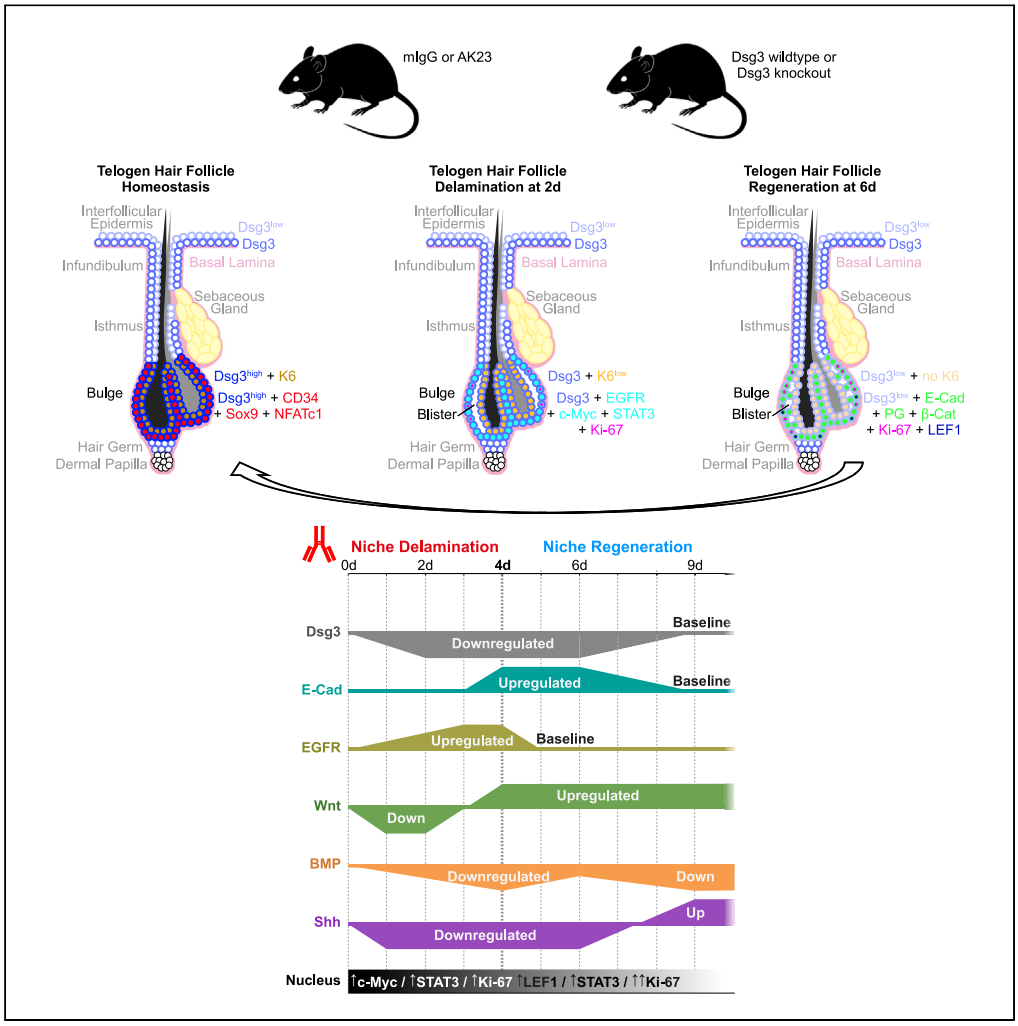

William V.J. Hariton, Katja Schulze, Siavash Rahimi, ..., Mỹ G. Mahoney, Arnaud Galichet, Eliane J. Müller

eliane.mueller@unibe.ch

Highlights

Dsg3 controls HF bulge SC quiescence through adhesion signaling (middle left)

Dsg3 inactivation triggers a self-organized regenerative program (top middle)

Activated HF bulge residents revert to the original quiescence and multipotency (top right)

HF bulge-relevant causative signaling networks feeds into transcriptional alterations (bottom)

Hariton et al., iScience *26*, 108568
December 15, 2023
https://doi.org/10.1016/j.isci.2023.108568

iScience

CellPress
OPEN ACCESS

Article

A desmosomal cadherin controls multipotent hair follicle stem cell quiescence and orchestrates regeneration through adhesion signaling

William V.J. Hariton,[1,2,3,4,7] Katja Schulze,[3,4,6,7] Siavash Rahimi,[1,2,3] Taravat Shojaeian,[1,2,3] Laurence Feldmeyer,[1] Roman Schwob,[3,4] Andrew M. Overmiller,[5] Beyza S. Sayar,[1,2,3] Luca Borradori,[1,3] Mỹ G. Mahoney,[5] Arnaud Galichet,[1,2,3,4] and Eliane J. Müller[1,2,3,4,8,*]

SUMMARY

Stem cells (SCs) are critical to maintain tissue homeostasis. However, it is currently not known whether signaling through cell junctions protects quiescent epithelial SC reservoirs from depletion during disease-inflicted damage. Using the autoimmune model disease pemphigus vulgaris (PV), this study reveals an unprecedented role for a desmosomal cadherin in governing SC quiescence and regeneration through adhesion signaling in the multipotent mouse hair follicle compartment known as the bulge. Autoantibody-mediated, mechanical uncoupling of desmoglein (Dsg) 3 transadhesion activates quiescent bulge SC which lose their multipotency and stemness, become actively cycling, and finally delaminate from their epithelial niche. This then initiates a self-organized regenerative program which restores Dsg3 function and bulge morphology including SC quiescence and multipotency. These profound changes are triggered by the sole loss of functional Dsg3, resemble major signaling events in *Dsg3−/−* mice, and are driven by SC-relevant EGFR activation and Wnt modulation requiring longitudinal repression of Hedgehog signaling.

INTRODUCTION

Understanding protective and regenerative mechanisms preventing mammalian SC reservoirs from disease- and age-related decline is a prerequisite to counter tissue degeneration.[1,2] To date, research on SC reservoirs has mostly focused on self-renewal, differentiation, and experimentally induced wound healing models, while the coordination of spontaneous regenerative processes in response to disease-inflicted damage is not well understood. Experimental models predicted that SCs sense injury through direct cell-cell contact as well as the contact with the microenvironment or "niche", able to coordinate regenerative processes.[3–5] However, the functional implication of SC cell-cell adhesion in general and through desmosomal cadherins in particular has remained elusive.

Desmosomal cadherins play a unique role in preserving tissue integrity by conveying strong intercellular adhesion. This cadherin family emerged late during metazoan evolution when tissues started to stratify and become more complex.[6] Accordingly, in mammals, desmosomal cadherins are expressed in tissues exposed to substantial mechanical stress such as epithelia (including their SC compartments) and the heart. The desmosomal cadherin family comprises desmogleins (Dsg1-4) and desmocollins (Dsc1-3) which are dynamically assembled into higher order adhesion structures, called desmosomes, in conjunction with their plaque proteins plakoglobin (JUP) and plakophilins.[7] Desmosomal cadherins vary in their expression in a tissue- and differentiation-specific pattern and, in stratified epithelia, they progressively increase in size and resilience from basal to suprabasal layers.

Beyond strong intercellular adhesion, desmosomes, desmosomal cadherins, as well as their plaque proteins are now also recognized to exhibit intrinsic signaling functions, thought to be indispensable for proper tissue homeostasis.[8–10] Comparable to adhesion molecules of the classical cadherin and integrin-types,[11,12] good evidence exists that desmosomal cadherins also exert mechanosensing and –signaling functions.[10,13,14] They were found to transmit mechanical forces to intermediate filaments but also to components related to the actin cytoskeleton such as Arp2/3, actomyosin or RhoA.[15–17] Accordingly, depending on the desmosomal cadherin subtype, dysfunction leads to severe disease

[1]Department of Dermatology, Inselspital, Bern University Hospital, University of Bern, 3010 Bern, Switzerland
[2]Department for BioMedical Research, Molecular Dermatology and Stem Cell Research, University of Bern, 3008 Bern, Switzerland
[3]DermFocus, Vetsuisse Faculty, University of Bern, 3008 Bern, Switzerland
[4]Institute of Animal Pathology, Vetsuisse Faculty, University of Bern, 3012 Bern, Switzerland
[5]Department of Dermatology and Cutaneous Biology, Thomas Jefferson University, Philadelphia, PA 19107, USA
[6]Present address: Genentech Inc., Roche, San Francisco, CA 94080, USA
[7]These authors contributed equally
[8]Lead contact
*Correspondence: eliane.mueller@unibe.ch
https://doi.org/10.1016/j.isci.2023.108568

manifestations and can even initiate tumor development and progression, which might occur prior to and independent of changes in classical cadherins present in adherens junctions.[18]

Pathogenic autoantibodies which specifically impair the function of Dsg3 or Dsg1 provide the opportunity to investigate the role of desmosomal cadherins in a singular way. These antibodies induce severe autoimmune blistering in stratified epithelia, known as PV and pemphigus foliaceus (PF), respectively.[19–21] Clinical blisters form at the site of highest relative expression and potentially main functional site of their antigenic target in a clinicopathological-relevant pattern: between basal and suprabasal layers in PV and in superficial layers in PF.[19,21,22] Accordingly, Dsg3 expression is highest in the basal cell layer harboring SCs, transit amplifying and committed progenitor cells while Dsg1 is increasingly expressed in suprabasal differentiating keratinocytes.

Alterations in signaling pathways upon uncoupling of Dsg3 transadhesion by PV antibodies suggested that Dsg3 receptors act as a signaling hub supporting differentiation, as mostly defined in 2D keratinocyte cultures at the transition between transit amplifying cells and committed precursors on their way to differentiate.[23,24] Accordingly, antibody-mediated Dsg3 uncoupling postpones the differentiation process resulting in increased proliferation[24,25] (also observed in PV patients) and enhanced migration.[26] However, although Dsg3 is also expressed in SCs of the epidermis and the multipotent reservoir of the hair follicle (HF), the signaling role of Dsg3 in SC biology is unknown.

Multiple models have been developed to study PV[23] of which the "adult PV mouse model" was specifically designed to investigate Dsg3 in the multipotent SC compartment of the HF, known as the telogen HF bulge (HFBu).[27] Unlike the widely used neonatal PV model, adult mice of young age present with finalized morphology of synchronously cycling HFs. This provides the opportunity to study the function of the desmosomal cadherin Dsg3 in a pure SC population of the quiescent, multipotent HFSC compartment. In this mouse model, subcutaneous injection of the experimental monospecific anti-Dsg3 antibody AK23[23,27,28] induces a clinicopathological phenotype like observed in mucosal-dominant PV patients characterized by anti-Dsg3 antibodies[21,22,29]: in the epidermis, blisters are restricted to quiescent telogen HFs, which express Dsg3 but no Dsg1 while sparing the interfollicular epidermis due to compensatory Dsg1 expression[22]; in the oral mucosa, without compensatory Dsg1, blisters form between the basal and suprabasal layer of the epithelium.[27] This blistering phenotype is also recapitulated in *Dsg3−/−* mice,[29] in which lesions in the quiescent HFBu appeared to have healed at onset of the next hair growth cycle at anagen stage. In contrast to the adult PV mouse model, used in this study, human skin organ cultures from hairy skin are not suited for longitudinal studies on Dsg3 in HFSCs because these cultures are rather short-lived and present with asynchronously cycling HFs as seen in humans.[29] The adult PV mouse model injected with the monospecific Dsg3 antibody AK23,[27] which specifically disrupts homophilic Dsg3-Dsg3 transadhesion (but not heterophilic Dsg3-Dsc3, Dsg3-Dsg2, Dsg3-Dsg1 or Dsc3-Dsg1 nor homophilic Dsg1-Dsg1 interactions[30–32]) in synchronously cycling HFs in the first and second HF cycle after birth, thus, represents an ideal tool to study local, Dsg3-dependent processes related to disease-inflicted insults in a homogeneous quiescent, multipotent SC compartment.

Our study of the multipotent telogen HFBu now reveals that Dsg3 has a major signaling role in safeguarding the quiescent HFSC reservoir from depletion by preventing SC activation. If Dsg3 function is compromised through antibody-mediated uncoupling or gene knockout, suppression of HFBu-specific pathways of SC quiescence is released, orchestrating a self-organized regenerative program before entering the next HF cycle. These findings identify a novel yet unrecognized function for desmosomal cadherins in SCs, with implications for cell fate modulatory plasticity and regenerative therapies also in other epithelia, and finally open new perspectives on druggable pathways in PV.

RESULTS

Uncoupling Dsg3 transadhesion initiates a stereotypic blistering and regeneration program in the quiescent HFBu

To study the role of Dsg3 in the multipotent stem cell reservoir of the HFBu, we functionally uncoupled Dsg3[30] by subcutaneous (s.c.) injection of AK23 antibody in four and eight-week-old C57BL/6J mice of the first or second synchronized telogen stage, respectively. Direct immunofluorescence microscopy revealed that the monospecific, pathogenic Dsg3 antibody mainly homes to the BuSCs and their keratin 6 positive (K6+), BuSC-supporting epithelial niche[33] (Figures 1A–1C), exclusively binding to and functionally affecting Dsg3 (Figures S1A and S1B). Antibody binding was visibly more moderate in the hair germ, poised to proliferate in the next HF cycle,[34] as well as in the continuously cycling interfollicular epidermis, recapitulating the Dsg3 expression pattern. AK23 binding equally affected the first and second telogen HFBu by inducing a biphasic response pattern; over four days, BuSC successively delaminated from the K6+ epithelial niche with apparent blisters in a zone of otherwise high desmosome density, followed by morphological repair (Figures 1B, 1D, and S1C). The biphasic blistering fate was reproduced in *Dsg3−/−* mice (Figures 1D and S1D).

In first telogen HFs with disrupted Dsg3 transadhesion or Dsg3 deletion, entry into the next hair cycle (anagen) was delayed until morphological repair was complete (Figures S1C and S1D). In the second telogen stage, which lasts multiple weeks, both mIgG and AK23 challenged HFs were still in telogen at the endpoint of repair (Figures 1B and 1D), providing the opportunity to conduct comparative molecular studies in the same HF stage. Immunofluorescence microscopy showed significantly reduced expression of both K6, typifying the epithelial HFBu niche,[33] and Dsg3. Concomitantly, Ki-67+ cells started to be expressed in the quiescent HFBu, marking induction of proliferation in a biphasic pattern, delineating the blistering and morphological repair phase, respectively. Expression of K6 and Dsg3 was only restored around day 9, when AK23 was cleared from the tissue, morphological repair completed and Ki-67 expression stopped (Figures 1B and 1D). Taken together, lack of Dsg3 function, either by antibody uncoupling or genetic deletion suggested that BuSCs lose their dormant nature and initiate a stereotypic program leading to morphological repair and restoration of niche architecture before entering the next HF cycle.

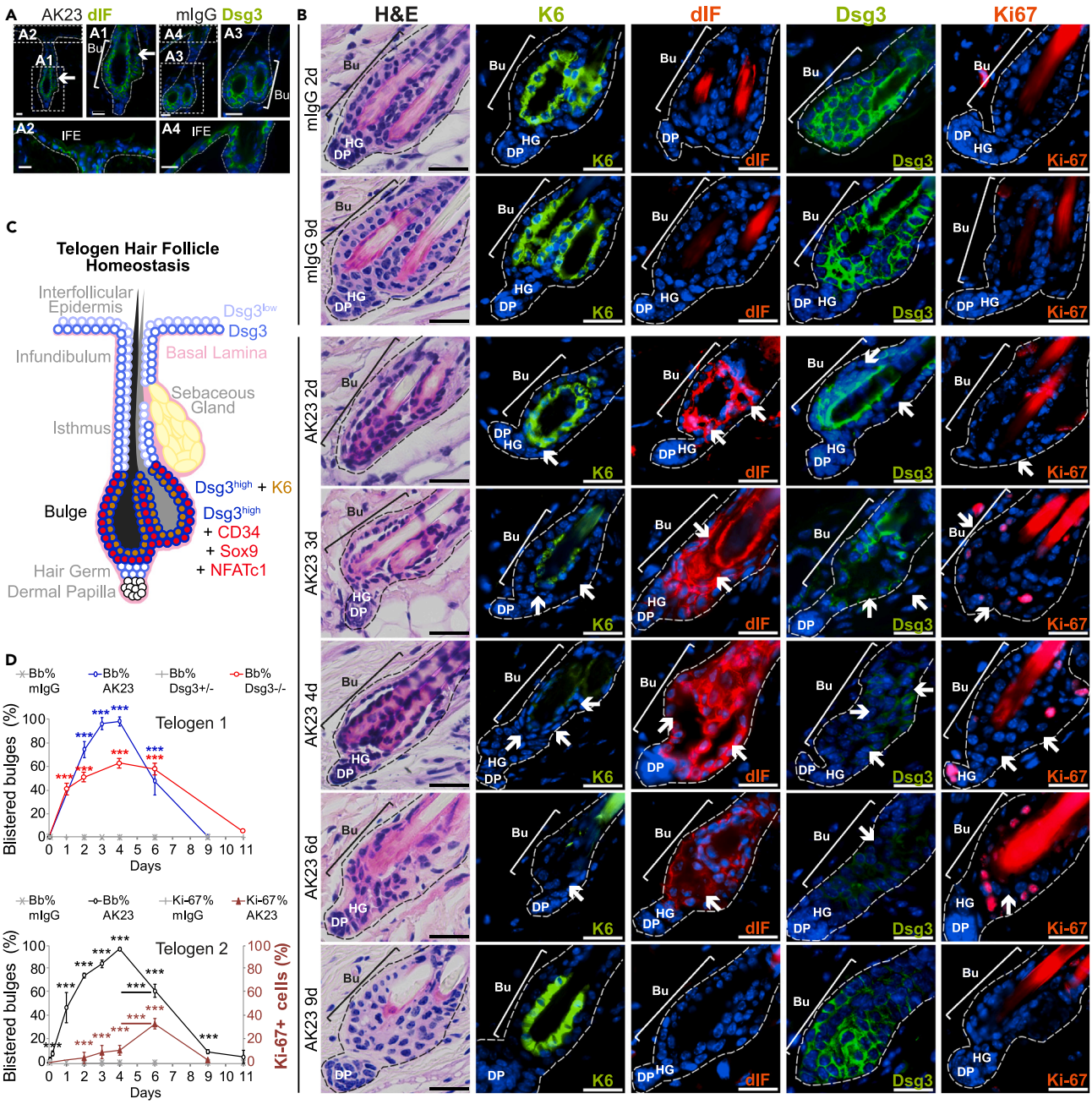

Figure 1. Delamination and regeneration in the telogen HFBu

(A and B) Immunolabeling and H&E of the telogen HFBu in 8-week-old C57BL/6J mice after a single s.c. injection of mIgG/AK23. Note that Dsg3 labeling is highest in the HFBu and low in HG and IFE. A1/3: telogen HFBu, A2/4: IFE: interfollicular epidermis, dIF: direct immunofluorescence detects bound AK23.

(C) Schematic representation of the mouse telogen HF. Dsg3 expression (dark blue) is strongest in the bulge. Specific SC markers CD34, Sox9 and NFATc1 (red, highlighted in this study) are expressed in the BuSC while K6 (brown) is expressed in the epithelial niche.[33]

(D) Longitudinal quantification of blistered HFBus (Bb). Top panel: First telogen C57BL/6J mice with single s.c. mIgG/AK23 injection (day 0, P20) or *Dsg3+/−* or *Dsg3−/−* mice (day 0, P18). Bottom panel: Second telogen C57BL/6J mice with single s.c. mIgG/AK23 injection (day 0, P56) and average % of Ki-67+ cells per HFBu. Shown are mean ± SEM. Data analyzed by a two-tailed Student's *t* test. ***p < 0.001.

(A and B) Dashed line indicates the HF. White arrows indicate blisters. Scale bars: 25 μm.

(A–C): IFE, interfollicular epidermis, SG, sebaceous gland, HG, hair germ, DP, dermal papilla.

(A, B, and D) per group, n ≥ 4 mice (except Dsg3 immunodetection mIgG/AK23, n = 3 mice).

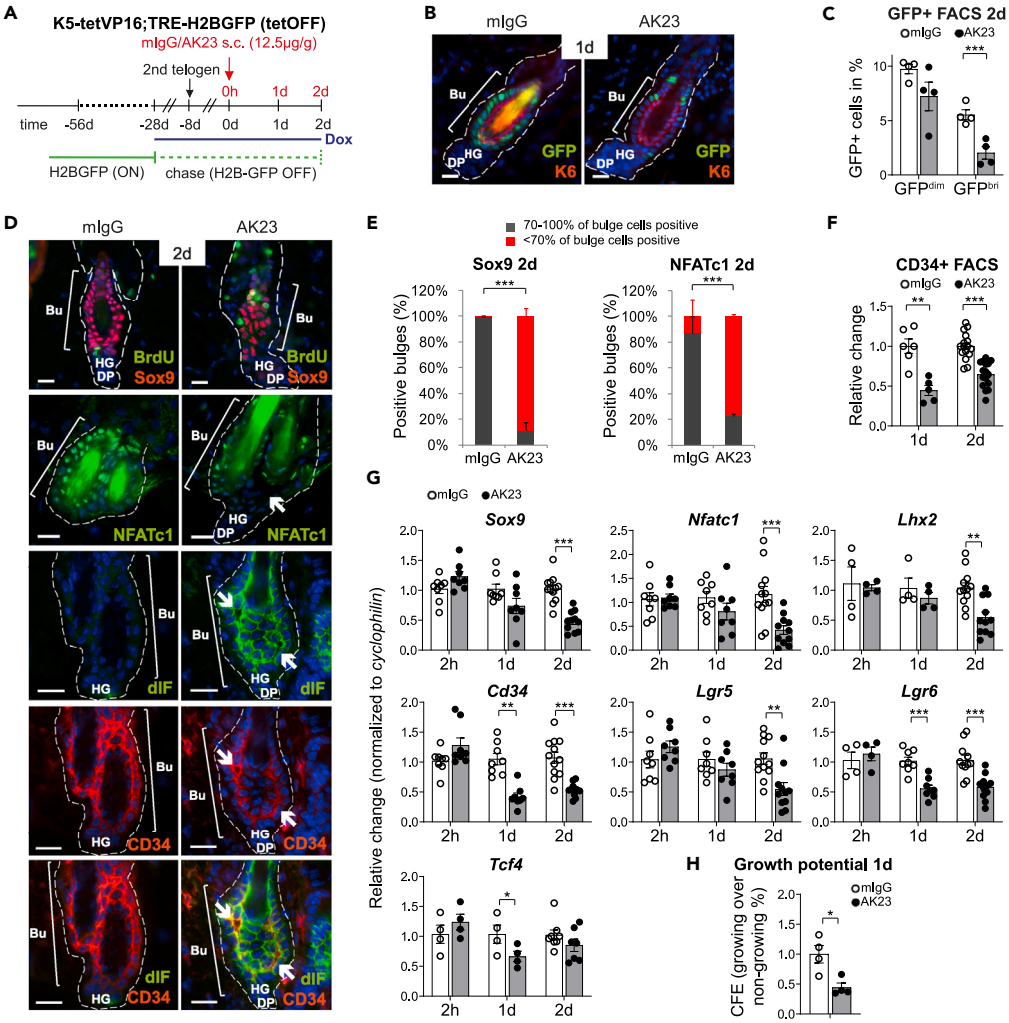

Figure 2. AK23 binding activates quiescent BuSCs losing their stemness signature

(A–C) Eight-week-old tetOFF H2BGFP mice after a 4-week chase and a single s.c. injection of mIgG/AK23. Label retaining cell (LRC) studies.

(A) Experimental outline to assess GFP+ LRCs 1 and 2 days after mIgG/AK23 injection.

(B) Immunodetection of GFP+ BuSCs and K6+ epithelial niche cells (red). Dashed line indicates the HF. AK23 treated mice already show fewer LRCs after 1 day.

(C) FACS quantification of isolated back skin keratinocytes gated for LIVE/DEAD-/CD31-/CD45-/GFPdim and GFPbri (bright) cells. Graph shows reduced GFPbri LRCs.

(D–H) Eight-week-old C57BL/6J mice after a single s.c. injection of mIgG/AK23.

(D) Immunodetection using indicated antibodies and BrdU incorporation in the HFBu. Note hair shaft (green) represents unspecific staining. Dashed line indicates the HF. White arrows indicate blisters.

(E) Quantification of Sox9 and NFATc1 positive cells per HFBu (>50 HFBus per group on random micrographs). Significances are indicated between the sum of positive HFBus in AK23 compared to mIgG mice.

(F) FACS of primary viable LIVE/DEAD-/CD31-/CD45-keratinocytes measured 1 and 2 days after treatment, gated for CD34. mIgG set to 1.

(G) RT-qPCR of HFBu markers assessed on back skin extracts relative to mIgG set to 1.

(H) Quantification of colony forming efficiency (CFE) of primary keratinocytes isolated 1day after mIgG/AK23 injection from back skin.

(A–H) per group, n ≥ 4 mice (except B n = 2), shown as mean ± SEM. Data analyzed by a two-tailed Student's *t* test. **p < 0.05, **p < 0.01, ***p < 0.001.

(B and D) Scale bars: 25µm.

Dsg3 transadhesion is required for BuSC quiescence

We confirmed *bona fide* loss of BuSC quiescence and BuSC activation upon Dsg3 uncoupling using doxycycline-repressible histone H2BGFP mice, which were developed to mark label-retaining BuSCs.[35] Already one day after AK23 injection, eight-week-old H2BGFP mice showed a marked reduction of the GFP bright (GFP^{bri}), suprabasal BuSCs in second telogen (Figures 2A–2C and S2A). Appearance of Ki-67+ cells in HFBus of AK23 injected C57BL/6J mice (Figures 1B and 1D) further temporally correlated with BrdU incorporation (Figure 2D).

The proliferative HF phenotype in AK23 injected C57BL/6J mice was accompanied by the successive loss of BuSC identity in terms of stemness marker expression. BuSC quiescence and maintenance protein markers,[36] Sox9, NFATc1 and the Bu-specific marker CD34 (Figures 2D–2F) were reduced in AK23-targeted HFBus, revealed by immunofluorescence microscopy. These markers as well as *Lhx2* also declined at the transcriptional level in back skin lysates from AK23 injected mice, shown by RT-qPCR (Figure 2G). Furthermore, as early as one day after AK23 injection, the same fate was seen for SC markers *Lgr5*, *Lgr6* and *Tcf4*, involved in Wnt signaling. Comparable to the break-down of compartmentalization during wound healing,[37] expression of markers of other skin SC compartments were also downregulated (Figure S2B), such as for example *Lrig1*, a suppressor of EGFR signaling in the junctional zone between the sebaceous gland and the infundibulum (Figure 1C).[36] Altered stemness upon Dsg3 uncoupling further resulted in a loss of long-term growth potential in a colony-forming efficiency assay. Already one day after AK23 injection, primary keratinocytes isolated from back skin of C57BL/6J mice, exhibited a 50% decrease in the ratio of growing to non-growing colonies ((BrdU+, Ki-67+, ΔNp63+ and involucrin$^-$ keratinocytes with high growth potential) over (involucrin+ keratinocytes with reduced growth potential)) (Figures 2H and S2C).

Collectively, these results demonstrate that uncoupling of Dsg3 transadhesion is sufficient to switch quiescent BuSC from resting to activated, proliferative HFBu residents. This is demonstrated by reduced stemness and impaired long-term growth potential, already prominent one day after AK23 injection. These characteristic features of activated BuSCs[33] identify Dsg3 as a gatekeeper of BuSC quiescence through transadhesion.

A self-organized program supports recovery of Dsg3, stemness and multipotency in the blistered HFBu

To address whether the AK23 exposed HFBu residents can recover BuSC identity and multipotency and regrow hair, grafting experiments were performed. Shaved back skin (to monitor new anagen growth) of second telogen CAG-EGFP mice was transplanted onto immunocompromised Swiss nude mice two days after mIgG/AK23 injection (Figure S3A). Comparable hair re-growth was observed after 35 and 56 days while histological examination showed a slight delay at day 35 in anagen downgrowth in AK23-treated skin (anagen IV in AK23 and anagen V in mIgG[38]). This delay was resolved by day 56, when both groups were in anagen V (Figure S3A). This suggested that blistered HFBus (Figure 1) had recovered from injury in an HF-autonomous regenerative process. The potential to self-recover multipotency was then addressed by the ability of isolated AK23 treated HFBu cells to reconstitute all epidermal lineages after pocket grafting.[39] One day after administering two consecutive high-dose mIgG/AK23 injections, primary keratinocyte suspensions were isolated from 8-week-old CAG-EGFP mice and grafted in a pocket of C57BL/6J mouse skin onto the back of Swiss nude mice (Figures 3A and S3B). A similar number of white donor hairs (CAG-EGFP) amidst black pocket hairs (C57BL/6J) were apparent in mIgG and AK23 groups at day25 and day77 post grafting (Figures 3A and S3C). Immunolabeling of grafts confirmed GFP+ donor cells to contribute to all epidermal lineages (HF, sebaceous glands (SG), interfollicular epidermis (IFE)) in both groups, indicating self-recovery of multipotency of AK23-targeted BuSCs (Figure 3B). Although the SC long-term growth potential was found to be significantly reduced after one day (Figure 2H), the grafting experiments demonstrated that the HFBu residents from AK23 injected mice are able to recover their multipotency. Full recovery of SC potential was also confirmed by a longitudinal colony forming efficiency assay of keratinocytes isolated from mIgG/AK23 treated C57BL/6J back skin (Figure 3C). Notably, the regenerative endpoint was marked by AK23 clearance (Figure 1B) and re-assembly of Dsg3-based desmosomes, confirmed by immunoblot analyses of Triton X-100 insoluble back skin lysates (Figure 3D). These events also engendered recovery of *Cd34* mRNA and CD34 surface protein (Figures 3E and 3F).

So far, these data demonstrate that transadhering Dsg3 is required to maintain HFSC quiescence. When transadhesion is lost, BuSCs swiftly initiate a stereotypic recovery program which implicates remarkable BuSC plasticity to regenerate the HFSC compartment. The velocity and reproducibility of this process suggested that transadhering Dsg3 receptors act by tight surveillance of a signaling network ranging from cell fate control (quiescence versus proliferation) to cell-cell adhesion.

Dsg3 surveys a relevant HFBu quiescence signaling network

If Dsg3 transadhesion functions as a gatekeeper, AK23-mediated uncoupling of Dsg3 was expected to affect the major signaling programs in control of telogen BuSC quiescence. Low Wnt and low Sonic hedgehog signaling (Shh) as well as high bone morphogenetic protein (BMP) levels are key footprints of quiescent BuSCs.[40–42] Moreover, EGFR signaling was recently demonstrated to be required to restrain Wnt signaling in postnatal telogen HFs to prevent unscheduled, Wnt-driven BuSC activation involving exhaustion of the BuSC pool.[43] Identifying the deregulation of these signaling pathways downstream of Dsg3 uncoupling and their potential implication in triggering the regenerative response was thus of relevance (addressed in the following subsections).

EGFR signaling is controlled by transadhering Dsg3

A significant increase in effectors of EFGR signaling was observed at day2, temporally coinciding with AK23-induced BuSC activation and the collective reduction in BuSC markers (Figures 2D–2G). These comprised PI3K/P-Akt-Ser473 and nuclear p-β-catenin-Ser552, detected in the HFBu by immunolabeling (Figure 4A) and immunoblotting of back skin lysates (Figure S4A). We thus addressed EGFR signal activation in AK23 treated animals longitudinally over the entire biphasic time course (Figure 1D). Combined HFBu immunolabeling and immunoblotting of back skin lysates revealed a stage-dependent activation of effectors in the EGFR signaling network downstream of loss of Dsg3 transadhesion, prominently marking the phases of niche delamination and regeneration (Figures 4A and 4B). Specifically, a decrease in EGFR protein levels by immunoblotting 2h after administering AK23 was followed by a prominent increase in EGFR expression observed around day3 in the HFBu by immunolabeling. This is compatible with stress-induced EGFR activation, receptor internalization and cell surface re-expression and

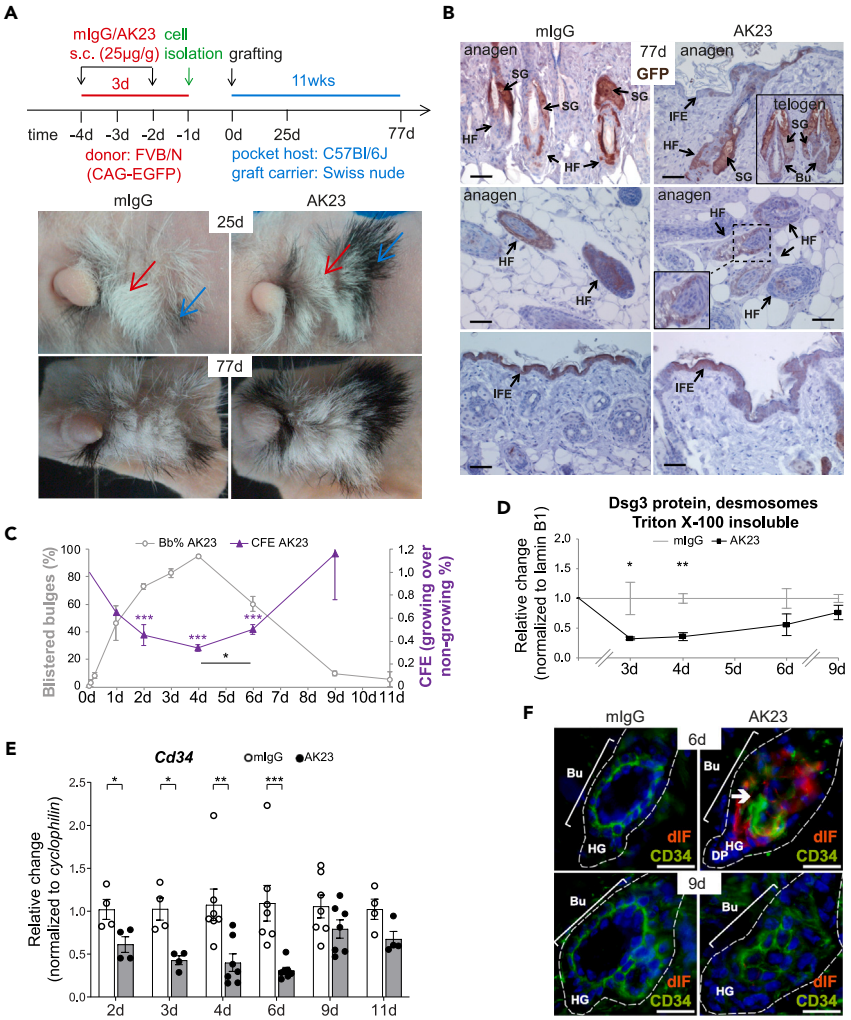

Figure 3. AK23 treated HFBu cells restore multipotency

(A and B) Eight-week-old CAG-EGFP mice received 2 s.c. injections of high dose mIgG/AK23.

(A) Epidermal reconstitution assay of SC lineages, experimental outline and macroscopic views. White hairs of the donor (CAG-EGFP; red arrows) are intermixed with black hairs of the pocket host (C57BL/6J; blue arrows) 25 and 77 days after grafting. Grafted cells on Swiss nude mice from mIgG and AK23 treated mice invariably grew white hair. Per group CAG-EGFP n = 2 mIgG; n = 3 AK23 mice; Swiss nude mice per group, n = 4 mice. See Figure S3C for complete set of mice.

(B) Immunohistochemistry of GFP+ cells on paraffin-embedded skin biopsies shows grafted GFP+ keratinocytes were present in all lineages; in sebaceous glans (SG), HFs including the HFBu, and interfollicular epidermis (IFE). Scale bars: 50µm.

(C–F) Eight-week-old C57BL/6J mice received 1 s.c. injection of mIgG/AK23.

(C) Quantification of blistered HFBu (from Figure 1C), in gray, and colony forming efficiency (CFE) assay relative to mIgG, in purple. Per group for CFE mIgG or AK23, 1 day n = 1; 2–9 days n = 3 mice.

(D) Graph represents quantitative immunoblot analyses of Dsg3 in Triton X-100 insoluble skin lysates (containing desmosomes) relative to mIgG set to 1.

(E) RT-qPCR of *Cd34* on back skin extracts relative to mIgG.

(F) Immunodetection of HFBu marker CD34 and direct immunofluorescence (dIF) at indicated time points. Dashed line indicates the HF. White arrow indicates blister. Scale bars: 25µm.

(D–F) per group, n ≥ 4 mice.

(A, C, and D) Data analyzed by a two-tailed Student's *t* test. *p < 0.05, **p < 0.01, ***p < 0.001. Graphs indicate mean ± SEM.

signaling, respectively.[44] Furthermore, STAT3 which can be activated downstream of EGFR or IL-6, and was implicated in stemness control, wound healing and HF neogenesis,[45] was sustainably upregulated. Remarkably, ERK1/2 and p38MAPK, effectors of the MAPK pathway as well as c-Myc, activated downstream of Tyr1173EGFR, Ras or Src or directly by uncoupled Dsg3, respectively,[24,46] synchronously peaked at day3 before onset of the regenerative process and were again significantly reduced by day4.

To highlight the causality of EGFR activation in the biphasic response program downstream of uncoupled Dsg3, we administered the dual EGFR/ErbB2 inhibitor lapatinib to C57BL/6J mice (Figure S4B); 4h before (to address EGFR causality in SC activation/delamination) or 4 and

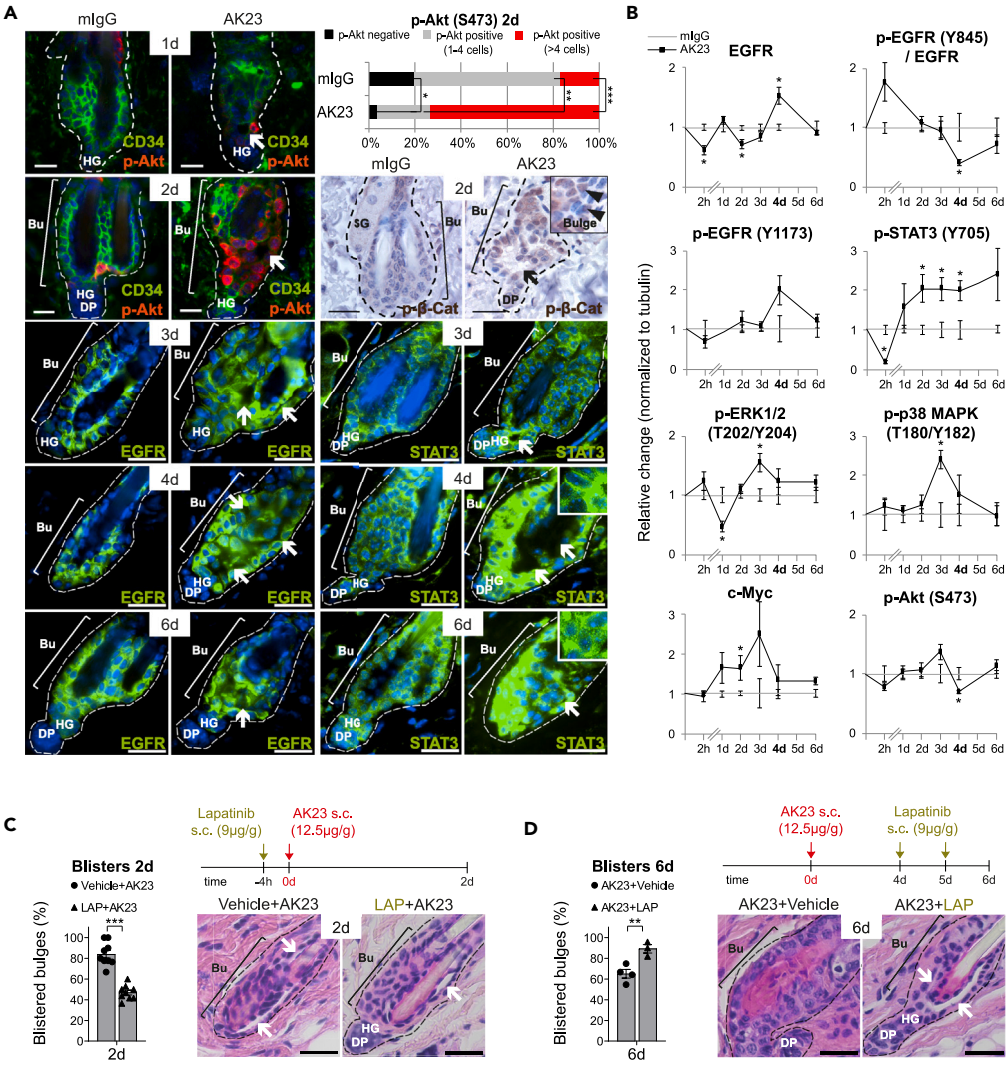

Figure 4. EGFR activation in the telogen HFBu

(A–D) Eight-week-old C57BL/6J mice received a single s.c. injection of mIgG/AK23.

(A) Quantification of *p*-Akt positive cells per HFBu (n = > 50 HFBus per group on random micrographs; significances are indicated between the sum of all *p*-Akt positive HFBus of AK23 compared to mIgG control) and immunodetection of EGFR and EGFR effectors, insets are lower exposure and zoomed in to show immunofluorescence pattern.

(B) Immunoblot analyses from back skin lysates, relative to mIgG set to 1 (gray line).

(C and D) EGFR inhibitor Lapatinib (LAP) treatment schemes, quantification of blistered HFBus and H&E.

(A, C and D) Dashed line indicates the HF. White arrows indicate blisters. Scale bars: 25µm. (A–D) per group, n ≥ 4 mice (except D n ≥ 3), shown as mean ± SEM. Data analyzed by a two-tailed Student's *t* test. *p < 0.05, **p < 0.01, ***p < 0.001.

5 days (to address EGFR causality in regeneration) after AK23 injection. Amelioration or worsening of endpoints, that is blistered HFBus, were monitored at day2 and day6, respectively. Lapatinib treatment 4h before AK23 injection reduced the size and number of blisters in HFBus on average by 50% (Figure 4C). In contrast, administering lapatinib at onset of morphological repair prevented healing of HFBu blisters as the number of blistered HFBu remained at the level when the drug was injected (day4) (Figure 4D). These results highlight the importance of functional Dsg3 transadhesion in preventing EGFR mis-activation in the quiescent HFBu.

Transadhering Dsg3 orchestrates Wnt signaling in the HFBu

In postnatal telogen HFBu, EGFR activation restrains canonical Wnt signaling,[43] preventing premature transition to the anagen stage.[47] As a consequence of EGFR activation and the delay in anagen entry in first telogen stage upon loss of Dsg3 transadhesion (Figures 4 and S1C), we expected reduced Wnt activity upon AK23 treatment. However, canonical Wnt also regulates self-renewal of epidermal keratinocytes,[48] suggesting a potential role of Wnt signaling in the regenerative process.

We used *Axin2*^{LacZ} mice expressing *LacZ* under the control of the Wnt-dependent *Axin2* promoter to address the status of Wnt signaling.[42,49] One day after mIgG/AK23 injection, no increase in Wnt levels, which are characteristically low in BuSCs, was detected in terms of Axin2-mediated *LacZ* expression (Figure 5A). The reduced steady-state mRNA levels of Wnt target genes *Lgr5, Lgr6* and *Sox9*, and of the transcription factor *Tcf4* at day1 and day2 (Figure 2G) suggested, however, that low level Wnt in the HFBu is diminished beyond detection. In contrast, Wnt signaling was activated at onset of regeneration when EGFR activity was on the decline (Figures 5A and 4B). This was shown by a 2.5-fold increase in *LacZ* levels measured at day6 after AK23 injection (Figure 5A). Consistently, nuclear accumulation of the Wnt-responsive transcription factor LEF1 was seen by immunolabeling with a peak at day4, when LEF1+ cells formed distinct clusters in the HFBu of AK23-treated C57BL/6J mice. LEF1 positive cells remained detectable through to day6 post AK23 injection (Figures 5B and 5C), contrasting with absence of LEF1 in HFBu of mIgG injected mice. Remarkably, the nuclear increase of LEF1 was initially observed in the hair germ before onset of morphological regeneration around day3. As AK23 did not detectably bind to the hair germ (Figures 1A and 1B), Wnt activation may occur in a paracrine fashion compatible with transcellular BuSC communication. In the same set of mice, we also addressed the fate of adherens junction components relating to Wnt signaling, E-cadherin, β-catenin and plakoglobin.[50] E-cadherin membrane localization was unaltered during the blistering phase until day2 (Figure S5). However, a visible increase in the expression levels of all adherens junction components was observed throughout the HFBu, including the hair germ, in the runup to the regenerative phase at day3 (Figure 5B). Compensational responses were further mirrored by increased transcriptional expression of E-cadherin (Figure 5D). These findings are compatible with the view that the cadherin/catenin complex can under specific circumstances positively regulate Wnt/β-catenin signaling, particularly in keratinocytes.[24,50]

To further address the causality of a biphasic Wnt signaling scheme for the events taking place downstream of uncoupled Dsg3 (Figures 5A–5C), we applied the specific Wnt activator BIO[51] 4/5 days after AK23 administration. Titration of BIO prior AK23 injection reduced blistering (Figure S4B), thus supporting the potential causative Wnt inhibition downstream of Dsg3 uncoupling, discussed above, and shown previously in epidermal keratinocytes.[24] Most importantly, injection of BIO at onset of regeneration (day4/5) aided morphological healing as this process became significantly accelerated (Figure 5E). In AK23-BIO-treated animals, less than 30% HFBus showed signs of small blisters at day6 compared to 65% full blown blistered HFBus in animals without BIO treatment. Remarkably, despite high Wnt, HFBus of BIO-treated animals remained in morphological telogen.

Taken together, Dsg3 transadhesion controls EGFR and Wnt signaling in telogen HFs as shown by AK23 treatment. Specifically, EGFR activation and Wnt inhibition are suggested here to be early, causative events in niche delamination. On the other hand, the process of morphological regeneration requires the subsequent activation of Wnt, which coincides with the gradual cessation of EGFR signaling around day6.

Inhibition of Sonic hedgehog (Shh) is a prerequisite for HFBu regeneration

Wnt activation in the regenerative phase downstream of uncoupled Dsg3 transadhesion failed to induce anagen entry (Figure 5), contrasting with homeostatic conditions.[47] To understand how second telogen BuSCs potentially escape anagen entry despite increased Wnt signaling, we first addressed whether the stereotypic delay in entering anagen, observed in the first telogen stage (Figure S1C), would also apply to the extended second telogen stage of AK23 injected mice. To this aim, anagen entry was forced by hair plucking[52] on the back of mice in second telogen, 2 days after AK23 injection (Figure 6A). At day9 after plucking, control animals showed the typical darkening of the skin, indicating hair regrowth.[52] This was absent from AK23-treated animals, demonstrating compromised anagen entry also in the second telogen stage.

We therefore investigated expression levels of two other drivers of anagen entry, Bmp and Shh, which are known to necessarily decrease and increase, respectively, when telogen BuSCs are activated and enter the next HF cycle.[40,41] Relative *Bmp2* mRNA expression levels were reduced in AK23-treated C57BL/6J mice over the entire time course up to day11 (Figure 6B). Reduced *Bmp2* levels are in line with BuSC activation and proliferation, elevated PI3K/Akt and reduced CD34 and NFATc1 levels,[41,53] observed here upon Dsg3 uncoupling (Figures 1D, 2A–2G, 4B, and S4A). Notwithstanding, both low BMP and high Wnt at day4 were not compatible with the delay in anagen entry outlined above (Figure 6A). In contrast, Hedgehog signaling was. The expression of the ligand *Shh* was reduced in AK23 treated animals over the entire time course up to day9 (Figure 6B). Furthermore, expression of the Shh receptor *Ptch1* and Shh target genes *Gli1* and *Gli2* was also diminished while *Sufu*, a negative regulator of hedgehog signaling, was unchanged (Figure S6A).

Forcing Shh activation on the background of activated Wnt at onset of regeneration (Figure 5) was anticipated to trigger anagen entry in AK23-injected mice.[40,41,47] Unexpectedly, however, SAG (Shh agonist) treatment of animals at day4/5, stalled morphological regeneration without driving HFs into anagen downgrowth (Figures 6C and S4B). Together these data demonstrate first that restricted Shh signaling is a prerequisite for HFBu regeneration to proceed, and second, suggest that intact desmosomal niche adhesion and its cross-talk to the BuSCs is a rate limiting step to proceed to the next HF cycle.

These observations were corroborated by our findings on *Dsg3−/−* mice in first telogen (Figure S1D). RT-qPCR performed on back skin lysates of these mice revealed that relative to *Dsg3+/−* mice, the delay in anagen entry was also accompanied by reduced Shh signaling (*Shh* and *Gli1*) (Figure 6D). Furthermore, a relative reduction of HFBu marker expression *CD34, Lhx2* and *Lgr5* and increase of Wnt signaling (*Wnt, Axin2, plakoglobin*) were also observed (Figure S6B), recapitulating the findings in AK23-injected mice (Figures 2G, 3E, and 5A). In contrast, relative levels of telogen-specific maintenance markers, *BMP* and *NFATc1*[41,53] were significantly increased in the short first telogen stage, lasting from P18 to P22 (Figures S6B and S1D). This finding is interesting as it aligns with the fact that the heterogeneous *Dsg3+/−* mice had already started their entry into anagen while the *Dsg3−/−* mice were still in full telogen (Figure S1D). It may also stem from adaptative measures due to the fact that lack of Dsg3 might trigger compensatory expression of other desmosomal cadherins. Importantly, however, once the blisters had healed in the *Dsg3−/−* mice, the delay in anagen entry (Figure S1C) was followed by the growth of a normal hair coat,[29] supporting regeneration like in AK23-treated mice.

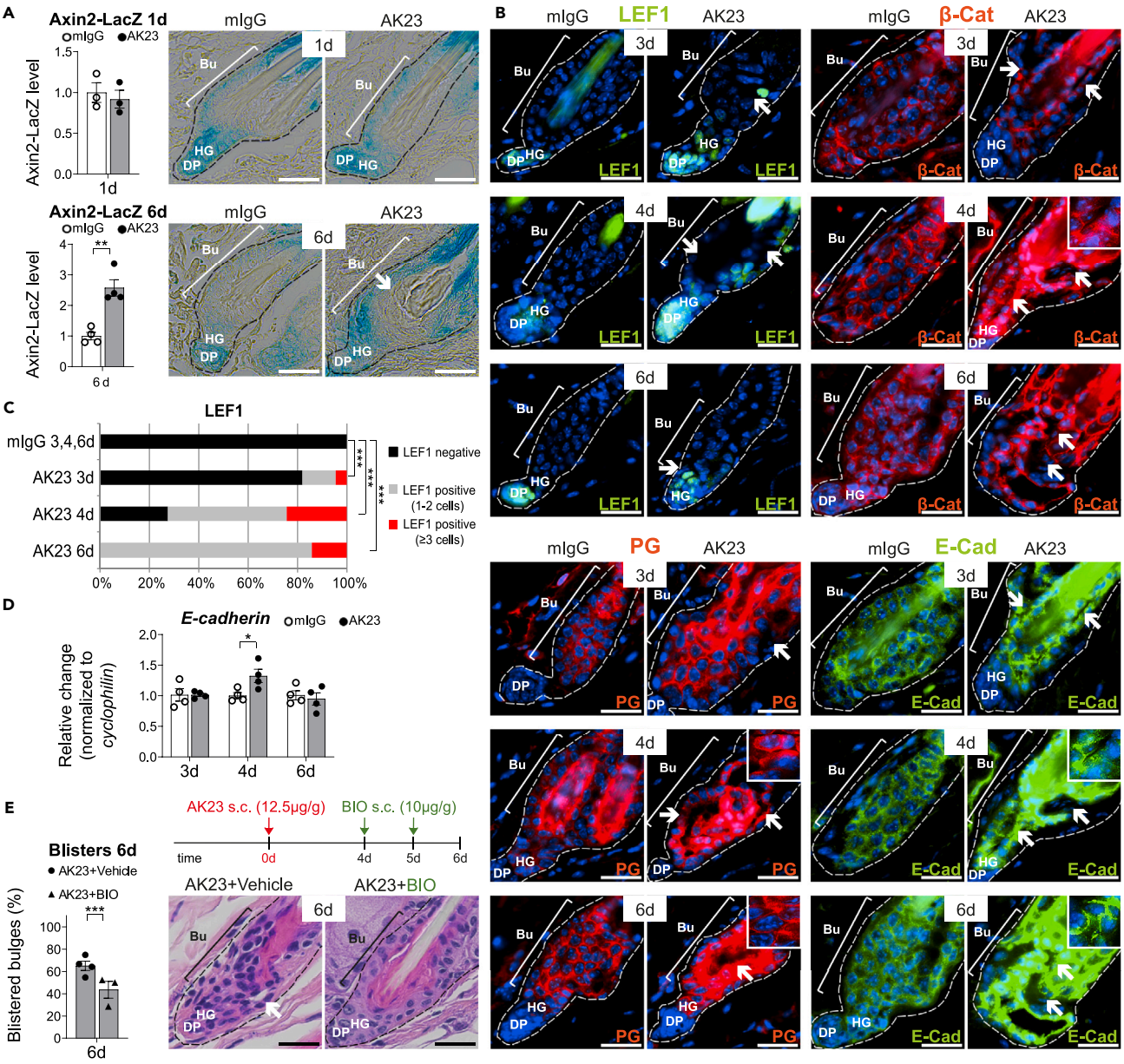

Figure 5. Wnt signaling in the telogen HFBu

(A) Eight-week-old Axin2-LacZ mice received a single s.c. injection of mIgG/AK23. X-Gal quantification on skin sections of Axin2-LacZ mice using ImageJ. mIgG set to 1.

(B–E) Eight-week-old C57BL/6J mice received a single s.c. injection of mIgG/AK23.

(B) Immunodetection of Wnt effectors and adherens junction components, insets are lower exposure and zoomed in to show immunofluorescence pattern. Abbreviations: β-Cat (β-catenin), PG (plakoglobin), E-Cad (E-cadherin).

(C) Quantification of LEF1 positive cells per HFBu (n = > 50 HFBus per group on random micrographs). Significances are indicated between the sum of all LEF1 positive HFBus of each AK23 time point compared to their respective mIgG controls.

(D) RT-qPCR of *E-cadherin* (*Cdh1*) on back skin extracts relative to mIgG.

(E) Wnt activator BIO treatment scheme, quantification of blistered HFBus and H&E.

(A, B, and E) Dashed line indicates the HF. White arrows indicate blisters. Scale bars: 25µm.

(A and E) per group, n ≥ 3 mice.

(B–D) per group, n ≥ 4 mice.

(A, D, and E) shown as mean ± SEM. Data analyzed by a two-tailed Student's *t* test. *p < 0.05, **p < 0.01, ***p < 0.001.

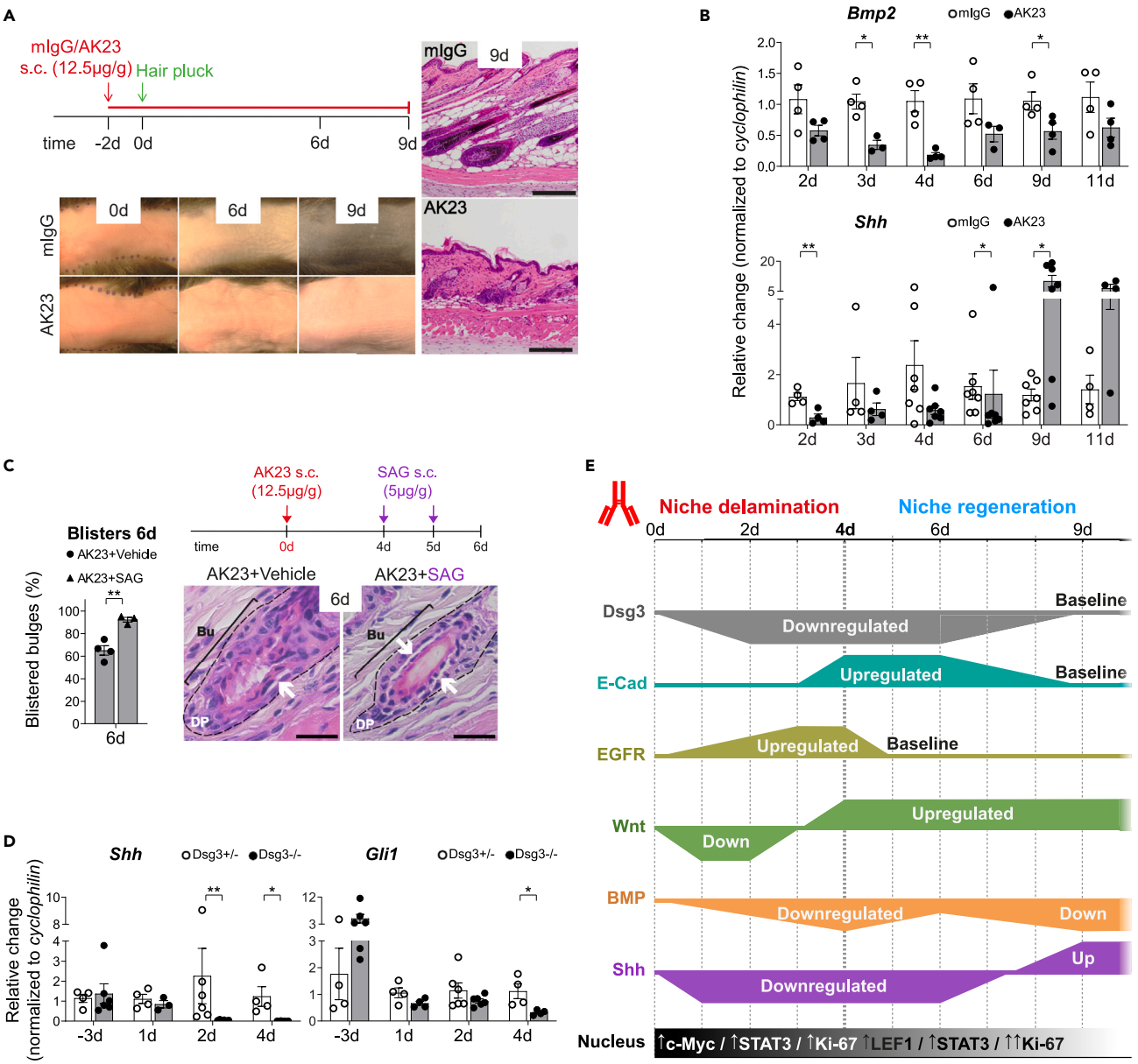

Figure 6. Delay in anagen entry/Shh suppression/Dsg3 governed signaling

(A–C) Eight-week-old C57BL/6J mice received a single s.c. injection of mIgG/AK23.

(A) Hair plucking: treatment scheme, macroscopic hair regrowth (left panel) and H&E (right panel). Hair re-growth (anagen entry) was delayed in AK23-treated mice. Scale bars: 50µm.

(B) RT-qPCR of *Bmp2* and *Shh* on back skin extracts relative to mIgG.

(C) Shh agonist SAG treatment scheme, quantification of blistered HFBus and H&E. Dashed line indicates the HF. White arrows indicate blisters. Scale bars: 25µm.

(D) First telogen *Dsg3+/−* or *Dsg3−/−* mice. RT-qPCR of *Shh* and *Gli1* on back skin extracts relative to *Dsg3+/−* mice.

(E) Schematic representation of Dsg3 protein levels in AK23 exposed HFBus. Relative activity of signaling pathways and nuclear proteins investigated in this study and consequences thereof.

(A–D) per group, n ≥ 3 mice.

(B, C, and D) shown as mean ± SEM. Data analyzed by a two-tailed Student's *t* test. *p < 0.05, **p < 0.01.

In conclusion, this study reveals that a desmosomal cadherin, represented here by Dsg3, has fundamental and unique properties in signal-mediated tissue surveillance beyond simple cell-cell adhesion. This comprises the control of HFSC quiescence and the orchestration of a stereotypic, regenerative program via signal modulation if Dsg3 function is compromised (Figure 6E).

DISCUSSION

On the evolutionary path to higher vertebrates, desmosomal cadherins emerged to uniquely protect tissue integrity from mechanical stress through knob-like, multimeric adhesion structures called desmosomes.[6,7] Uncoupling Dsg3 transadhesion or Dsg3 deletion in the multipotent HFBu investigated here now reveals that the role of desmosomal cadherins to preserve tissue integrity reaches beyond current concepts; first, functional Dsg3 is required at the core of tissue renewal and homeostasis, this is to preserve the SC reservoir; second, the function of Dsg3 is to couple extracellular adhesion to an intricate intracellular signaling network in surveillance of key pathways keeping SC quiescence in check; and third, if Dsg3 function is lost through uncoupling transadhesion, a potent stereotypic program, including fate conversion of quiescent SCs and blistering, is kicked off to restore desmosomal adhesion, SC quiescence, and niche integrity. The majority of these findings is also recapitulated in *Dsg3*−/− mice. Taken together, Dsg3 is demonstrated here to act as a gatekeeper and sensor of tissue integrity in its function as a regulator of SC quiescence-specific pathways through adhesion-signaling (Figure 6E).

Extra-desmosomal (Triton X-100 soluble) Dsg3, which was initially identified as plasma membrane precursor *en route* for desmosome assembly,[54] was found to be the main target of transadhesion disrupting AK23 antibodies.[19] In analogy to thermodynamic principles of ligand-induced receptor activation described for example for integrin signaling,[55] altered Dsg3 signaling likely occurs through conformational changes of Dsg3 receptors upon antibody binding and disruption of extracellular transadhesion.[30,55] A conformational change can then for example activate the signal transducer and Dsg3 plaque protein plakoglobin, previously shown to modulate nuclear Wnt signaling downstream of uncoupled Dsg3.[25] If Dsg3 is deleted, lack of plakoglobin stabilization at the plasma membrane conceivably results in a similar phenotype than Dsg3 uncoupling, including decreased nuclear Wnt signaling during blister formation and increased Wnt signaling as part of tissue regeneration.[24,25]

Injury-dependent tissue regeneration can re-activate developmental signaling programs as occurring during wound healing.[56] Here we demonstrate that disruption of Dsg3 transadhesion in the second telogen HFBu provides a fast forward signal for EGFR activation and Wnt inhibition driving a "pathological" response including fate conversion and blistering (Figures 1, 2, 4, and 5). Remarkably, the integration of high EGFR and low Wnt signaling was recently revealed as a key signaling network to preserve the BuSC pool during post-natal HF morphogenesis.[43] In contrast to kinase-inactive EGFR mice, reported in the former study, Dsg3 uncoupling reported here additionally inhibits Shh signaling (Figure 6). A crosstalk of compromised Dsg3 function to Shh was further confirmed in *Dsg3*−/− mice (Figure 6C). Dsg3 might thus directly surveil Shh signaling (Figures 6B–6D and S6). Although this possibility requires further investigations on the nature of such a molecular crosstalk, lack of functional Dsg3 also impacts Wnt signaling in the BuSCs (Figure 5). A feedback loop between hedgehog and canonical Wnt was reported in HFBu morphogenesis and basal cell carcinomas,[57] potentially further aligning Dsg3 function with important developmental patterns. In addition to these patterns of HF morphogenesis highlighted during the blistering phase in AK23 treated animals, the regenerative phase also unveiled signaling patterns of *de novo* HF growth.[45] This is, HF neogenesis was demonstrated to activate Wnt and STAT3, similarly as revealed here (Figures 3 and 6E). However, HF neogenesis requires Shh signaling to instruct the dermis to invaginate and initiate the HF downgrowth.[58] If the HFBu is not lost but injured, suppression of Shh signaling on the background of high Wnt and STAT3 may indeed be a fail-safe mechanism to favor HF regeneration over HF neogenesis. In conclusion, the discovery that disrupting Dsg3 or Dsg3 deletion influences key signaling pathways associated with HF morphogenesis and regeneration underscores the significance of the role of Dsg3 in maintaining HFBu morphology and BuSCs quiescence while preserving the BuSC population (Figure 3). When Dsg3 function is compromised, a self-regulating signaling network is activated to restore the integrity and multipotency of HFBu through conserved mechanisms and extensive BuSCs plasticity.

SC plasticity has been described as a characteristic measure serving adaptive purposes.[59] Comparable plasticity and return to the original multipotency and lineage commitment, as described here (Figure 3), have been demonstrated in experimental models of skin, the crypt in the gut, and in particular for hematopoietic SCs. The process includes a switch from the quiescent state to activation and back to quiescence to re-establish homeostasis after injury[56,60,61] such as uncovered here. The similarity between the self-organized program of HFBu SCs and other SC compartments suggests that the identified regenerative process of the BuSCs follows a conserved pattern. As a consequence, the loss of Dsg3 governed pathways may more broadly apply to wounding and other tissue damage in stratified epithelia implicating adhesive signaling through Dsg3 and potentially Dsc3, co-expressed in the HFBu.[62] In simple epithelia, other desmosomal cadherins such as Dsg2, which also modulate mitogenic activities,[63] might orchestrate similar processes if their function is lost.

The profound alterations in BuSC biology implicating fate conversion after Dsg3 uncoupling, highlighted in this study, were not reported in case of conditional deletion of E-cadherin in BuSCs,[64–66] and E-cadherin was not affected in the blistering phase of AK23 injected mice (Figure S5). This is compatible with the recent finding that plasma membrane confinement of the adherens junction protein E-cadherin and desmosomal cadherin Dsg1 segregate from each other under homeostatic conditions.[15] However, an elegant study recently involved E− and P-cadherin (but not desmosomal cadherins) in crowding-associated, tension-dependent fate conversion in mouse interfollicular epidermis at onset of differentiation and stratification.[67] Because the expression of desmosomal cadherins is compromised upon simultaneous deletion of E− and P-cadherin,[68] as applied by the authors,[67] a contribution of desmosomal cadherins in epidermal fate conversion toward stratification cannot be excluded and has indeed been highlighted recently for Dsg1.[15,69] Similarly, when E-cadherin is not only deleted in BuSCs but also in the P-cadherin negative, epithelial K6+ niche of the telogen HFBu, a "breach" in niche adhesion and focal proliferative events were observed.[64] Although the proliferative phenotype was tied to T cell infiltrates, T cells have no impact in the current model. This was shown by *bona fide* niche delamination/blistering after the injection of AK23 into *Rag2*−/− mice.[27] It is thus possible that simultaneous deletion of E− and P-cadherin in HFBu affects niche-restricted expression of Dsg3 or Dsc3 receptors leading to proliferative events, seen in the second, regenerative phase of our model (Figures 1 and 6E). Our findings thus generally suggest that models on cell-cell adhesion-dependent epithelial and skin appendage homeostasis warrant inclusion of analyses on desmosomal cadherin expression such as Dgs2, Dsg3, Dsc3 and in the epidermis also Dsg1, which can inhibit EGFR signaling through Erbin.[70]

In spite of the fact that a cross-talk exists between classical and desmosomal cadherins and their respective adhesion components,[68,71] it is of further interest that Dsg3 and Dsc3, which are the major desmosomal cadherins expressed in the quiescent HFBu,[62] have been assigned intrinsic regulatory functions potentially influencing, but not depending, on E-cadherin. In a seminal study, early embryonic lethality of Dsc3 null mutant mice was observed before compaction, the formation of mature desmosomes and E-cadherin protein expression.[72] This led the authors to conclude that Dsc3 receptors can exert key signaling functions in absence of E-cadherin. A similar conclusion was drawn from a developmental mouse model of mammary luminal epithelium where transadhesion-disrupting peptides to both Dsg3 and Dsc3 were sufficient to abrogate cell positioning without functionally affecting nor involving E-cadherin.[73] Furthermore, although studies on BuSC activation upon disruption of Dsc3 transadhesion are not available, conditional Dsc3 genetic deletion in mouse skin also resulted in PV-like HF blisters.[62] Functional independence of desmosomal cadherins from classical cadherins under conditions of tissue surveillance was also suggested by investigations on epithelial tumor development where desmosomal cadherins were found to act as tumor suppressors and gate keepers of tissue integrity, and desmosomal dysfunction preceded that of adherens junctions in cancer progression.[18] These findings are consistent with the present study, where major alterations in E-cadherin were confined to the second, regenerative phase (Figure 5). It also aligns with the fact that the desmosomal cadherin network has evolved into a highly specialized form to preserve tissue integrity[6] which cannot be mechanically compensated for by classical cadherins. This suggests a model whereby Dsg3 and other desmosomal cadherins act as primary sensors to the malfunction of cell-cell adhesion to protect SCs in injured tissue through a fail-safe mechanism of tissue blistering and regeneration such as described in this study. On the basis of homophilic rather than heterophilic (Dsc3/Dsg3) transadhesion highlighted by mechanistic studies in PV,[30] these collective findings not only assign key regulatory functions to Dsg3 and Dsc3 independently of each other but also independently of a primary contribution of classical cadherins.

Delamination/blistering is a well-known clinical readout in the epidermis and oral mucosa of PV patients.[19,21,74] However, the ability of the tissue to self-repair PV blisters and the implication of SC activation has not been recognized so far. Unlike mice, humans have asynchronously cycling HFs, rendering HF blisters less apparent. If patients are left untreated and infections involve SC death, it cannot be excluded that BuSCs are progressively exhausted resulting in alopecia in the long-term. This is supported by the observation that progressive hair loss is known to clinicians as a feature of PV patients.[75] Unlike the well protected BuSC niche, epidermis and oral mucosa are more exposed and prone to mechanical abrasion. This may render the blistering phenotype in these tissues more severe and might have been masking the existence of SC-mediated regenerative processes. Some similarity in signaling pathway activation and the site of blistering in the HF compared to the deep epidermis or oral mucosa points toward the possibility that SC activation also applies to other sites in PV. Accordingly, knowledge gained in this study on therapeutics preventing PV pathology may also be relevant to treat epidermal and mucous membrane blistering (Figure 6E). Above all, our study highlights that pharmacological treatment of patients needs to be selected with caution. Some drugs will compromise the formation of new blisters but concomitantly prevent existing lesions from healing, as shown here for example in presence of EGFR inhibitors (Figures 4C and 4D). In contrast, Wnt activation prevents blistering and enhances repair and healing (Figures S2B and 5). Local Wnt activation might therefore be considered as a first line topical therapy approach for treatment of PV patients, also for epidermal blisters,[24] along with drugs that have the same asymmetric response pattern reported here for Wnt (Figure 6E). Our results also lay the groundwork for novel adhesion modulatory strategies altering epithelial SC fate in regenerative and tumor biology. As described herein, loss of transadhesion is the primary signal to induce rapid proliferation and activate a regenerative program restoring multipotency through extensive plasticity. In early epidermal tumors, similarities between cancer cells and normal BuSC are seen and HFBu-derived $CD34^+$ cells were proposed as a source for tumorigenesis.[76] In hematopoietic SC, cadherin-based adhesion was discussed as a potential target for niche manipulation to decrease the SC niche interaction and overcome resistance to chemotherapy targeting cycling cells.[77] Such an approach might now also apply for desmosomal cadherins.

In conclusion, our work provides a detailed description of a mechanism that controls HFBu SC quiescence and orchestrates niche regeneration through loss of desmosomal cadherin transadhesion and function. The stipulated role for Dsg3 orchestrating a BuSC regenerative signaling network (Figure 6E), represents a paradigm shift underlying novel approaches into epithelial tissue homeostasis and cell fate modulatory strategies by taking into account an "adhesion code"[78,79] which includes desmosomal cadherins. This likely applies to PV and possibly other blistering diseases and has the potential to innovate approaches in regenerative medicine and epithelial cancer therapies.

Limitations of the study

The limitations of the current study are two-fold. The comparable clinico-morphological PV blistering phenotype of HF, epidermis, and mucous membranes suggests that Dsg3 uncoupling, although uncovered here in HF SCs, is also affecting SCs in stratified epithelia. This question will need to be addressed to understand whether pemphigus vulgaris is a SC activating disease in general. The latter is challenging, however, due to poor characterization of SCs and a mix of SCs, transit amplifying and committed progenitor cells in basal epithelia. Such studies are, therefore, preferentially conducted in cultured human keratinocytes in which these different populations can be better distinguished. Second, the desmosomal cadherin family comprises various other members of adhesion molecules, such as Dsg2 or Dsc3, which have not been addressed here, and will require other mouse models to define their potential role in epithelial SCs.

STAR★METHODS

Detailed methods are provided in the online version of this paper and include the following:

- KEY RESOURCES TABLE

SUPPLEMENTAL INFORMATION

Supplemental information can be found online at https://doi.org/10.1016/j.isci.2023.108568.

ACKNOWLEDGMENTS

We thank the ITPA Histology Lab, the Microscopy Imaging Center and LCI Core Facility of the University of Bern for their services. We thank Drs. Anne Wilson, Ilaria Malanchi, Stephanie Claudinot, and Ariane Rochat for kindly teaching flow cytometry, cell isolation, single cell grafting and clonal growth assay. We are thankful to Profs Kathleen Green and Fiona Watt for comments on the manuscript and Simon Broad (Fiona Watt lab) for fruitful technical advice. We are indebted to Profs Ralf Ludwig and Mariana Ricca for critically reading the manuscript. We kindly thank researchers that provided mouse strains and antibodies for the studies, and Dr Masa Amagai for the AK23 hybridoma. We acknowledge financial support from "Coordination Theme I (Health) of the European Community's FP7, grant agreement number, HEALTH-F2-2008-200515", Swiss National Science Foundation grants #31003A_135689, #CRSII3_160738, #CFII5 301202, Hans Sigrist Foundation (W.V.J.H.), Novartis Biomedical Research Fund (K.S.) and Martha Stiftung Zürich, Switzerland.

AUTHOR CONTRIBUTIONS

W.V.J.H., K.S, A.G., R.S., S.R., T.S., and L.F. conducted/contributed to the experiments with exception of Dsg3 immunofluorescence microscopy which was performed by M.G.M. and A.M.O. E.J.M., K.S., A.G., W.V.J.H., and B.S.S. designed the study. E.J.M., W.V.J.H., K.S., M.B.M., and L.B. wrote and edited the manuscript.

Co-first authors: K.S. performed initial experiments on blistering/delamination and W.V.J.H. on regeneration. W.V.J.H. finalized the study.

DECLARATION OF INTERESTS

The last author (E.J.M.) is a founder and director of the board of CELLnTEC Advanced Cell Systems AG. We used CELLnTEC media in this study. All other authors have declared no conflict of interest.

Received: September 6, 2023
Revised: November 3, 2023
Accepted: November 21, 2023
Published: November 25, 2023

REFERENCES

1. Brunet, A., Goodell, M.A., and Rando, T.A. (2023). Ageing and rejuvenation of tissue stem cells and their niches. Nat. Rev. Mol. Cell Biol. *24*, 45–62.

2. Oh, J., Lee, Y.D., and Wagers, A.J. (2014). Stem cell aging: mechanisms, regulators and therapeutic opportunities. Nat. Med. *20*, 870–880.

3. Chen, S., Lewallen, M., and Xie, T. (2013). Adhesion in the stem cell niche: biological roles and regulation. Development *140*, 255–265.

4. Wagers, A.J. (2012). The stem cell niche in regenerative medicine. Cell Stem Cell *10*, 362–369.
5. Lane, S.W., Williams, D.A., and Watt, F.M. (2014). Modulating the stem cell niche for tissue regeneration. Nat. Biotechnol. *32*, 795–803.
6. Green, K.J., Roth-Carter, Q., Niessen, C.M., and Nichols, S.A. (2020). Tracing the Evolutionary Origin of Desmosomes. Curr. Biol. *30*, R535–R543.
7. Getsios, S., Huen, A.C., and Green, K.J. (2004). Working out the strength and flexibility of desmosomes. Nat. Rev. Mol. Cell Biol. *5*, 271–281.
8. Müller, L., Hatzfeld, M., and Keil, R. (2021). Desmosomes as Signaling Hubs in the Regulation of Cell Behavior. Front. Cell Dev. Biol. *9*, 745670.
9. Müller, E.J., Williamson, L., Kolly, C., and Suter, M.M. (2008). Outside-in signaling through integrins and cadherins: a central mechanism to control epidermal growth and differentiation? J. Invest. Dermatol. *128*, 501–516.
10. Rubsam, M., Broussard, J.A., Wickstrom, S.A., Nekrasova, O., Green, K.J., and Niessen, C.M. (2017). Adherens Junctions and Desmosomes Coordinate Mechanics and Signaling to Orchestrate Tissue Morphogenesis and Function: An Evolutionary Perspective. Cold Spring Harbor Perspect. Biol. *10*, a029207.
11. Hannezo, E., and Heisenberg, C.P. (2019). Mechanochemical Feedback Loops in Development and Disease. Cell *178*, 12–25.
12. Miroshnikova, Y.A., and Wickström, S.A. (2022). Mechanical Forces in Nuclear Organization. Cold Spring Harb. Perspect. Biol. *14*, a039685.
13. Green, K.J., Niessen, C.M., Rübsam, M., Perez White, B.E., and Broussard, J.A. (2022). The Desmosome-Keratin Scaffold Integrates ErbB Family and Mechanical Signaling to Polarize Epidermal Structure and Function. Front. Cell Dev. Biol. *10*, 903696.
14. Broussard, J.A., Yang, R., Huang, C., Nathamgari, S.S.P., Beese, A.M., Godsel, L.M., Hegazy, M.H., Lee, S., Zhou, F., Sniadecki, N.J., et al. (2017). The desmoplakin-intermediate filament linkage regulates cell mechanics. Mol. Biol. Cell *28*, 3156–3164.
15. Nekrasova, O., Harmon, R.M., Broussard, J.A., Koetsier, J.L., Godsel, L.M., Fitz, G.N., Gardel, M.L., and Green, K.J. (2018). Desmosomal cadherin association with Tctex-1 and cortactin-Arp2/3 drives perijunctional actin polymerization to promote keratinocyte delamination. Nat. Commun. *9*, 1053.
16. Sumigray, K., Zhou, K., and Lechler, T. (2014). Cell-cell adhesions and cell contractility are upregulated upon desmosome disruption. PLoS One *9*, e101824.
17. Waschke, J., Spindler, V., Bruggeman, P., Zillikens, D., Schmidt, G., and Drenckhahn, D. (2006). Inhibition of Rho A activity causes pemphigus skin blistering. J. Cell Biol. *175*, 721–727.
18. Dusek, R.L., and Attardi, L.D. (2011). Desmosomes: new perpetrators in tumour suppression. Nat. Rev. Cancer *11*, 317–323.
19. Di Zenzo, G., Amber, K.T., Sayar, B.S., Müller, E.J., and Borradori, L. (2016). Immune response in pemphigus and beyond: progresses and emerging concepts. Semin. Immunopathol. *38*, 57–74.
20. Stanley, J.R., and Amagai, M. (2008). Autoimmune Bullous Diseases: Historical Perspectives. J. Invest. Dermatol. *128*, E16–E18.
21. Hammers, C.M., and Stanley, J.R. (2016). Mechanisms of Disease: Pemphigus and Bullous Pemphigoid. Annu. Rev. Pathol. *11*, 175–197.
22. Mahoney, M.G., Wang, Z., Rothenberger, K., Koch, P.J., Amagai, M., and Stanley, J.R. (1999). Explanations for the clinical and microscopic localization of lesions in pemphigus foliaceus and vulgaris. J. Clin. Invest. *103*, 461–468.
23. Hartmann, V., Hariton, W.V., Rahimi, S., Hammers, C.M., Ludwig, R.J., Müller, E.J., and Hundt, J.E. (2023). The human skin organ culture model as an optimal complementary tool for murine pemphigus models. Lab. Anim. *57*, 381–395.
24. Williamson, L., Raess, N.A., Caldelari, R., Zakher, A., de Bruin, A., Posthaus, H., Bolli, R., Hunziker, T., Suter, M.M., and Müller, E.J. (2006). Pemphigus vulgaris identifies plakoglobin as key suppressor of c-Myc in the skin. EMBO J. *25*, 3298–3309.
25. Williamson, L., Hunziker, T., Suter, M.M., and Müller, E.J. (2007). Nuclear c-Myc: a molecular marker for early stage pemphigus vulgaris. J. Invest. Dermatol. *127*, 1549–1555.
26. Rötzer, V., Hartlieb, E., Winkler, J., Walter, E., Schlipp, A., Sardy, M., Spindler, V., and Waschke, J. (2016). Desmoglein 3-Dependent Signaling Regulates Keratinocyte Migration and Wound Healing. J. Invest. Dermatol. *136*, 301–310.
27. Schulze, K., Galichet, A., Sayar, B.S., Scothern, A., Howald, D., Zymann, H., Siffert, M., Zenhäusern, D., Bolli, R., Koch, P.J., et al. (2012). An adult passive transfer mouse model to study desmoglein 3 signaling in pemphigus vulgaris. J. Invest. Dermatol. *132*, 346–355.
28. Tsunoda, K., Ota, T., Aoki, M., Yamada, T., Nagai, T., Nakagawa, T., Koyasu, S., Nishikawa, T., and Amagai, M. (2003). Induction of pemphigus phenotype by a mouse monoclonal antibody against the amino-terminal adhesive interface of desmoglein 3. J. Immunol. *170*, 2170–2178.
29. Koch, P.J., Mahoney, M.G., Cotsarelis, G., Rothenberger, K., Lavker, R.M., and Stanley, J.R. (1998). Desmoglein 3 anchors telogen hair in the follicle. J. Cell Sci. *111*, 2529–2537.
30. Heupel, W.M., Zillikens, D., Drenckhahn, D., and Waschke, J. (2008). Pemphigus vulgaris IgG directly inhibit desmoglein 3-mediated transinteraction. J. Immunol. *181*, 1825–1834.
31. Spindler, V., Heupel, W.M., Efthymiadis, A., Schmidt, E., Eming, R., Rankl, C., Hinterdorfer, P., Müller, T., Drenckhahn, D., and Waschke, J. (2009). Desmocollin 3-mediated binding is crucial for keratinocyte cohesion and is impaired in pemphigus. J. Biol. Chem. *284*, 30556–30564.
32. Sigmund, A.M., Steinert, L.S., Egu, D.T., Bayerbach, F.C., Waschke, J., and Vielmuth, F. (2020). Dsg2 Upregulation as a Rescue Mechanism in Pemphigus. Front. Immunol. *11*, 581370.
33. Hsu, Y.C., Pasolli, H.A., and Fuchs, E. (2011). Dynamics between Stem Cells, Niche, and Progeny in the Hair Follicle. Cell *144*, 92–105.
34. Greco, V., Chen, T., Rendl, M., Schober, M., Pasolli, H.A., Stokes, N., Dela Cruz-Racelis, J., and Fuchs, E. (2009). A two-step mechanism for stem cell activation during hair regeneration. Cell Stem Cell *4*, 155–169.
35. Tumbar, T., Guasch, G., Greco, V., Blanpain, C., Lowry, W.E., Rendl, M., and Fuchs, E. (2004). Defining the epithelial stem cell niche in skin. Science *303*, 359–363.
36. Kretzschmar, K., and Watt, F.M. (2014). Markers of epidermal stem cell subpopulations in adult mammalian skin. Cold Spring Harb. Perspect. Med. *4*, a013631.
37. Dekoninck, S., and Blanpain, C. (2019). Stem cell dynamics, migration and plasticity during wound healing. Nat. Cell Biol. *21*, 18–24.
38. Paus, R., Müller-Röver, S., Van Der Veen, C., Maurer, M., Eichmüller, S., Ling, G., Hofmann, U., Foitzik, K., Mecklenburg, L., and Handjiski, B. (1999). A comprehensive guide for the recognition and classification of distinct stages of hair follicle morphogenesis. J. Invest. Dermatol. *113*, 523–532.
39. Claudinot, S., Nicolas, M., Oshima, H., Rochat, A., and Barrandon, Y. (2005). Long-term renewal of hair follicles from clonogenic multipotent stem cells. Proc. Natl. Acad. Sci. USA *102*, 14677–14682.
40. Sato, N., Leopold, P.L., and Crystal, R.G. (1999). Induction of the hair growth phase in postnatal mice by localized transient expression of Sonic hedgehog. J. Clin. Invest. *104*, 855–864.
41. Kobielak, K., Stokes, N., de la Cruz, J., Polak, L., and Fuchs, E. (2007). Loss of a quiescent niche but not follicle stem cells in the absence of bone morphogenetic protein signaling. Proc. Natl. Acad. Sci. USA *104*, 10063–10068.
42. Lim, X., Tan, S.H., Yu, K.L., Lim, S.B.H., and Nusse, R. (2016). Axin2 marks quiescent hair follicle bulge stem cells that are maintained by autocrine Wnt/beta-catenin signaling. Proc. Natl. Acad. Sci. USA *113*, E1498–E1505.
43. Tripurani, S.K., Wang, Y., Fan, Y.X., Rahimi, M., Wong, L., Lee, M.H., Starost, M.F., Rubin, J.S., and Johnson, G.R. (2018). Suppression of Wnt/beta-catenin signaling by EGF receptor is required for hair follicle development. Mol. Biol. Cell *29*, 2784–2799.
44. Talukdar, S., Emdad, L., Das, S.K., and Fisher, P.B. (2020). EGFR: An essential receptor tyrosine kinase-regulator of cancer stem cells. Adv. Cancer Res. *147*, 161–188.
45. Bhoopalam, M., Garza, L.A., and Reddy, S.K. (2020). Wound Induced Hair Neogenesis - A Novel Paradigm for Studying Regeneration and Aging. Front. Cell Dev. Biol. *8*, 582346.
46. Berkowitz, P., Hu, P., Warren, S., Liu, Z., Diaz, L.A., and Rubenstein, D.S. (2006). p38MAPK inhibition prevents disease in pemphigus vulgaris mice. Proc. Natl. Acad. Sci. USA *103*, 12855–12860.
47. Lien, W.H., Polak, L., Lin, M., Lay, K., Zheng, D., and Fuchs, E. (2014). In vivo transcriptional governance of hair follicle stem cells by canonical Wnt regulators. Nat. Cell Biol. *16*, 179–190.
48. Lim, X., and Nusse, R. (2013). Wnt signaling in skin development, homeostasis, and disease. Cold Spring Harb. Perspect. Biol. *5*, a008029.
49. Lustig, B., Jerchow, B., Sachs, M., Weiler, S., Pietsch, T., Karsten, U., van de Wetering, M., Clevers, H., Schlag, P.M., Birchmeier, W., and Behrens, J. (2002). Negative feedback loop of Wnt signaling through upregulation of conductin/axin2 in colorectal and liver tumors. Mol. Cell Biol. *22*, 1184–1193.
50. McCrea, P.D., Maher, M.T., and Gottardi, C.J. (2015). Nuclear signaling from cadherin adhesion complexes. Curr. Top. Dev. Biol. *112*, 129–196.
51. Meijer, L., Skaltsounis, A.L., Magiatis, P., Polychronopoulos, P., Knockaert, M., Leost, M., Ryan, X.P., Vonica, C.A., Brivanlou, A.,

Dajani, R., et al. (2003). GSK-3-selective inhibitors derived from Tyrian purple indirubins. Chem. Biol. *10*, 1255–1266.
52. Müller-Röver, S., Handjiski, B., van der Veen, C., Eichmüller, S., Foitzik, K., McKay, I.A., Stenn, K.S., and Paus, R. (2001). A comprehensive guide for the accurate classification of murine hair follicles in distinct hair cycle stages. J. Invest. Dermatol. *117*, 3–15.
53. Horsley, V., Aliprantis, A.O., Polak, L., Glimcher, L.H., and Fuchs, E. (2008). NFATc1 balances quiescence and proliferation of skin stem cells. Cell *132*, 299–310.
54. Pasdar, M., and Nelson, W.J. (1988). Kinetics of desmosome assembly in Madin-Darby canine kidney epithelial cells: temporal and spatial regulation of desmoplakin organization and stabilization upon cell-cell contact. II. Morphological analysis. J. Cell Biol. *106*, 687–695.
55. Campbell, I.D., and Humphries, M.J. (2011). Integrin structure, activation, and interactions. Cold Spring Harb. Perspect. Biol. *3*, a004994.
56. Sun, X., Joost, S., and Kasper, M. (2023). Plasticity of Epithelial Cells during Skin Wound Healing. Cold Spring Harb. Perspect. Biol. *15*, a041232.
57. Yang, S.H., Andl, T., Grachtchouk, V., Wang, A., Liu, J., Syu, L.J., Ferris, J., Wang, T.S., Glick, A.B., Millar, S.E., and Dlugosz, A.A. (2008). Pathological responses to oncogenic Hedgehog signaling in skin are dependent on canonical Wnt/beta3-catenin signaling. Nat. Genet. *40*, 1130–1135.
58. Lim, C.H., Sun, Q., Ratti, K., Lee, S.H., Zheng, Y., Takeo, M., Lee, W., Rabbani, P., Plikus, M.V., Cain, J.E., et al. (2018). Hedgehog stimulates hair follicle neogenesis by creating inductive dermis during murine skin wound healing. Nat. Commun. *9*, 4903.
59. Clevers, H., and Watt, F.M. (2018). Defining Adult Stem Cells by Function, Not by Phenotype. Annu. Rev. Biochem. *87*, 1015–1027.
60. Wilson, A., Laurenti, E., Oser, G., van der Wath, R.C., Blanco-Bose, W., Jaworski, M., Offner, S., Dunant, C.F., Eshkind, L., Bockamp, E., et al. (2008). Hematopoietic stem cells reversibly switch from dormancy to self-renewal during homeostasis and repair. Cell *135*, 1118–1129.
61. van Es, J.H., Sato, T., van de Wetering, M., Lyubimova, A., Yee Nee, A.N., Gregorieff, A., Sasaki, N., Zeinstra, L., van den Born, M., Korving, J., et al. (2012). Dll1+ secretory progenitor cells revert to stem cells upon crypt damage. Nat. Cell Biol. *14*, 1099–1104.
62. Ganeshan, R., Chen, J., and Koch, P.J. (2010). Mouse models for blistering skin disorders. Dermatol. Res. Pract. *2010*, 584353.
63. Brennan, D., Hu, Y., Joubeh, S., Choi, Y.W., Whitaker-Menezes, D., O'Brien, T., Uitto, J., Rodeck, U., and Mahoney, M.G. (2007). Suprabasal Dsg2 expression in transgenic mouse skin confers a hyperproliferative and apoptosis-resistant phenotype to keratinocytes. J. Cell Sci. *120*, 758–771.
64. Lay, K., Kume, T., and Fuchs, E. (2016). FOXC1 maintains the hair follicle stem cell niche and governs stem cell quiescence to preserve long-term tissue-regenerating potential. Proc. Natl. Acad. Sci. USA *113*, E1506–E1515.
65. Tinkle, C.L., Lechler, T., Pasolli, H.A., and Fuchs, E. (2004). Conditional targeting of E-cadherin in skin: insights into hyperproliferative and degenerative responses. Proc. Natl. Acad. Sci. USA *101*, 552–557.
66. Lay, K., Yuan, S., Gur-Cohen, S., Miao, Y., Han, T., Naik, S., Pasolli, H.A., Larsen, S.B., and Fuchs, E. (2018). Stem cells repurpose proliferation to contain a breach in their niche barrier. Elife *7*, e41661.
67. Miroshnikova, Y.A., Le, H.Q., Schneider, D., Thalheim, T., Rübsam, M., Bremicker, N., Polleux, J., Kamprad, N., Tarantola, M., Wang, I., et al. (2018). Adhesion forces and cortical tension couple cell proliferation and differentiation to drive epidermal stratification. Nat. Cell Biol. *20*, 69–80.
68. Michels, C., Buchta, T., Bloch, W., Krieg, T., and Niessen, C.M. (2009). Classical cadherins regulate desmosome formation. J. Invest. Dermatol. *129*, 2072–2075.
69. Hegazy, M., Koetsier, J.L., Huffine, A.L., Broussard, J.A., Godsel, B.M., Cohen-Barak, E., Sprecher, E., Wolfgeher, D.J., Kron, S.J., Godsel, L.M., and Green, K.J. (2022). Epidermal stratification requires retromer-mediated desmoglein-1 recycling. Dev. Cell *57*, 2683–2698.e8.
70. Harmon, R.M., Simpson, C.L., Johnson, J.L., Koetsier, J.L., Dubash, A.D., Najor, N.A., Sarig, O., Sprecher, E., and Green, K.J. (2013). Desmoglein-1/Erbin interaction suppresses ERK activation to support epidermal differentiation. J. Clin. Invest. *123*, 1556–1570.
71. Lechler, T., and Fuchs, E. (2007). Desmoplakin: an unexpected regulator of microtubule organization in the epidermis. J. Cell Biol. *176*, 147–154.
72. Den, Z., Cheng, X., Merched-Sauvage, M., and Koch, P.J. (2006). Desmocollin 3 is required for pre-implantation development of the mouse embryo. J. Cell Sci. *119*, 482–489.
73. Runswick, S.K., O'Hare, M.J., Jones, L., Streuli, C.H., and Garrod, D.R. (2001). Desmosomal adhesion regulates epithelial morphogenesis and cell positioning. Nat. Cell Biol. *3*, 823–830.
74. Schmidt, E., Kasperkiewicz, M., and Joly, P. (2019). Pemphigus. Lancet *394*, 882–894.
75. Veraitch, O., Ohyama, M., Yamagami, J., and Amagai, M. (2013). Alopecia as a rare but distinct manifestation of pemphigus vulgaris. J. Eur. Acad. Dermatol. Venereol. *27*, 86–91.
76. Malanchi, I., Peinado, H., Kassen, D., Hussenet, T., Metzger, D., Chambon, P., Huber, M., Hohl, D., Cano, A., Birchmeier, W., and Huelsken, J. (2008). Cutaneous cancer stem cell maintenance is dependent on beta-catenin signalling. Nature *452*, 650–653.
77. Hosokawa, K., Arai, F., Yoshihara, H., Iwasaki, H., Hembree, M., Yin, T., Nakamura, Y., Gomei, Y., Takubo, K., Shiama, H., et al. (2010). Cadherin-based adhesion is a potential target for niche manipulation to protect hematopoietic stem cells in adult bone marrow. Cell Stem Cell *6*, 194–198.
78. Steinberg, M.S. (1970). Does differential adhesion govern self-assembly processes in histogenesis? Equilibrium configurations and the emergence of a hierarchy among populations of embryonic cells. J. Exp. Zool. *173*, 395–433.
79. Tsai, T.Y.C., Sikora, M., Xia, P., Colak-Champollion, T., Knaut, H., Heisenberg, C.P., and Megason, S.G. (2020). An adhesion code ensures robust pattern formation during tissue morphogenesis. Science *370*, 113–116.
80. Li, E.R., Owens, D.M., Djian, P., and Watt, F.M. (2000). Expression of involucrin in normal, hyperproliferative and neoplastic mouse keratinocytes. Exp. Dermatol. *9*, 431–438.
81. Paladini, R.D., Takahashi, K., Bravo, N.S., and Coulombe, P.A. (1996). Onset of re-epithelialization after skin injury correlates with a reorganization of keratin filaments in wound edge keratinocytes: defining a potential role for keratin 16. J. Cell Biol. *132*, 381–397.
82. Stolt, C.C., Lommes, P., Sock, E., Chaboissier, M.C., Schedl, A., and Wegner, M. (2003). The Sox9 transcription factor determines glial fate choice in the developing spinal cord. Genes Dev. *17*, 1677–1689.
83. Di Iorio, E., Barbaro, V., Ruzza, A., Ponzin, D., Pellegrini, G., and De Luca, M. (2005). Isoforms of DeltaNp63 and the migration of ocular limbal cells in human corneal regeneration. Proc. Natl. Acad. Sci. USA *102*, 9523–9528.
84. Rheinwald, J.G., and Green, H. (1975). Serial cultivation of strains of human epidermal keratinocytes: the formation of keratinizing colonies from single cells. Cell *6*, 331–343.
85. Diamond, I., Owolabi, T., Marco, M., Lam, C., and Glick, A. (2000). Conditional gene expression in the epidermis of transgenic mice using the tetracycline-regulated transactivators tTA and rTA linked to the keratin 5 promoter. J. Invest. Dermatol. *115*, 788–794.
86. Schindelin, J., Arganda-Carreras, I., Frise, E., Kaynig, V., Longair, M., Pietzsch, T., Preibisch, S., Rueden, C., Saalfeld, S., Schmid, B., et al. (2012). Fiji: an open-source platform for biological-image analysis. Nat. Methods *9*, 676–682.
87. Caldelari, R., and Müller, E.J. (2010). Short- and long-term cultivation of embryonic and neonatal murine keratinocytes. Methods Mol. Biol. *633*, 125–138.
88. Anhalt, G.J., Till, G.O., Diaz, L.A., Labib, R.S., Patel, H.P., and Eaglstein, N.F. (1986). Defining the role of complement in experimental pemphigus vulgaris in mice. J. Immunol. *137*, 2835–2840.
89. de Bruin, A., Caldelari, R., Williamson, L., Suter, M.M., Hunziker, T., Wyder, M., and Müller, E.J. (2007). Plakoglobin-dependent disruption of the desmosomal plaque in pemphigus vulgaris. Exp. Dermatol. *16*, 468–475.
90. Jensen, K.B., Driskell, R.R., and Watt, F.M. (2010). Assaying proliferation and differentiation capacity of stem cells using disaggregated adult mouse epidermis. Nat. Protoc. *5*, 898–911.
91. Barrandon, Y., and Green, H. (1987). Three clonal types of keratinocyte with different capacities for multiplication. Proc. Natl. Acad. Sci. USA *84*, 2302–2306.
92. Ito, M., Liu, Y., Yang, Z., Nguyen, J., Liang, F., Morris, R.J., and Cotsarelis, G. (2005). Stem cells in the hair follicle bulge contribute to wound repair but not to homeostasis of the epidermis. Nat. Med. *11*, 1351–1354.
93. Caldelari, R., de Bruin, A., Baumann, D., Suter, M.M., Bierkamp, C., Balmer, V., and Müller, E. (2001). A central role for the armadillo protein plakoglobin in the autoimmune disease pemphigus vulgaris. J. Cell Biol. *153*, 823–834.

STAR★METHODS

KEY RESOURCES TABLE

REAGENT or RESOURCE	SOURCE	IDENTIFIER
Antibodies		
Rat monoclonal anti-CD31 for FACS (1:100 dilution)	eBioscience	Cat#13-0311-82; RRID: AB_466420
Rat monoclonal anti-CD34 for FACS (1:100 dilution)	eBioscience	Cat#11-0341-85; RRID: AB_465022
Rat monoclonal anti-CD45 for FACS (1:100 dilution)	eBioscience	Cat#13-0451-82; RRID: AB_466446
Rat monoclonal anti-α6 Integrin for FACS (1:100 dilution)	eBioscience	Cat#555735; RRID: AB_396078
Rabbit polyclonal anti-Beta-Tubulin for immunoblot (1:10,000 dilution)	Abcam	Cat#ab6046; RRID: AB_2210370
Rabbit polyclonal anti-c-Myc for immunoblot (1:500 dilution)	Cell Signaling Technology	Cat#9402S; RRID: AB_2151827
Rabbit polyclonal anti-Desmoglein 3 for immunoblot (1:3,000 dilution)	J. Stanley, gift	Koch et al.[29] #3069
Rabbit polyclonal anti-EGFR for immunoblot (1:1,000 dilution)	Millipore	Cat#06-847; RRID: AB_2096607
Rabbit polyclonal anti-Lamin B1 for immunoblot (1:2,000 dilution)	Abcam	Cat#ab16048; RRID: AB_443298
Rabbit polyclonal anti-p-Akt (Ser473) for immunoblot (1:1,000 dilution)	Cell Signaling Technology	Cat#9271S; RRID: AB_329825
Rabbit polyclonal anti-p-β-Catenin (Ser552) for immunoblot (1:1,000 dilution)	Cell Signaling Technology	Cat#9566S; RRID: AB_1031116
Mouse monoclonal anti-p-EGFR (Tyr1173) for immunoblot (1:500 dilution)	Millipore	Cat#05-483; RRID: AB_309754
Rabbit polyclonal anti-p-EGFR (Tyr845) for immunoblot (1:500 dilution)	Cell Signaling Technology	Cat#2231S; RRID: AB_1264155
Rabbit polyclonal anti-p-ERK1/2 (Thr202/Tyr204) for immunoblot (1:1,000 dilution)	Cell Signaling Technology	Cat#9101S; RRID: AB_331646
Rabbit polyclonal anti-p-p38 MAPK (Thr180/Tyr182) for immunoblot (1:1,000 dilution)	Cell Signaling Technology	Cat#9211S; RRID: AB_331641
Rabbit polyclonal anti-PI3K p85 N-SH2 domain for immunoblot (1:1,000 dilution)	Millipore	Cat#ABS233; RRID: AB_2722790
Rabbit monoclonal anti-p-PTEN (Ser380/Thr382/Thr383) for immunoblot (1:1,000 dilution)	Cell Signaling Technology	Cat#9549S; RRID: AB_659891
Rabbit polyclonal anti-p-STAT3 (Tyr705) for immunoblot (1:500 dilution)	Cell Signaling Technology	Cat#9131S; RRID: AB_331586
Rat monoclonal anti-BrdU for immunolabeling (1:100 dilution)	Abcam	Cat#ab6326; RRID: AB_305426
Rat monoclonal anti-CD34 for immunolabeling (1:100 dilution)	BD Biosciences	Cat#553731; RRID: AB_395015

(*Continued on next page*)

Continued

REAGENT or RESOURCE	SOURCE	IDENTIFIER
Rabbit polyclonal anti-Desmoglein 3 for immunolabeling (1:100 dilution)	J. Stanley, gift	Koch et al.[29] #AP904
Goat polyclonal anti-Mouse IgG for immunolabeling (1:200 dilution)	Thermo Fisher Scientific	Cat#A-21125; RRID: AB_2535767
Rabbit monoclonal anti-E-Cadherin for immunolabeling (1:200 dilution)	Cell Signaling Technology	Cat#3195S; RRID: AB_2291471
Rabbit polyclonal anti-EGFR for immunolabeling (1:600 dilution)	Millipore	Cat#06-847; RRID: AB_2096607
Rabbit polyclonal anti-GFP for immunolabeling (1:50 dilution)	Molecular Probes	Cat#A11122; RRID: AB_221569
Rabbit monoclonal anti-Involucrin for immunolabeling (1:80 dilution)	F. Watt, gift	Li et al.[80] #ERLI-3
Rabbit polyclonal anti-K6 for immunolabeling (1:200 dilution)	P. Coulombe, gift	Paladini and Coulombe[81]
Rabbit monoclonal anti-Ki67 for immunolabeling (1:100 dilution)	Cell Marque	Cat#275R-15; RRID: AB_1158033
Rabbit monoclonal anti-LEF1 for immunolabeling (1:200 dilution)	Cell Signaling Technology	Cat#2230S; RRID: AB_823558
Mouse monoclonal anti-NFATc1 for immunolabeling (1:10 dilution)	Santa Cruz	Cat#SC-7294; RRID: AB_2152503
Rabbit polyclonal anti-p-Akt (Ser473) for immunolabeling (1:25 dilution)	Cell Signaling Technology	Cat#9271S; RRID: AB_329825
Rabbit polyclonal anti-p-β-Catenin (Ser552) for immunolabeling (1:1,000 dilution)	Cell Signaling Technology	Cat#9566S; RRID: AB_1031116
Mouse monoclonal anti-PG (γ-Catenin) for immunolabeling (1:150 dilution)	BD Biosciences	Cat#610254; RRID: AB_2629499
Rabbit polyclonal anti-Sox9 for immunolabeling (1:2,000 dilution)	M. Wegner, gift	Stolt et al.[82]
Rabbit monoclonal anti-Stat3 for immunolabeling (1:200 dilution)	Cell Signaling Technology	Cat#12640S; RRID: AB_2629499
Mouse monoclonal anti-β-Catenin for immunolabeling (1:500 dilution)	Sigma-Aldrich	Cat#C7207; RRID: AB_476865
Rabbit polyclonal anti-ΔNp63 for immunolabeling (1:100 dilution)	M. De Luca, gift	Di Iorio et al.[83]
Goat anti-Mouse IgG (H + L) Cross-Adsorbed Secondary Antibody, Alexa Fluor 488 (1:200 dilution)	Invitrogen	Cat#A11001; RRID: AB_2534069
Goat anti-Rabbit IgG (H + L) Highly Cross-Adsorbed Secondary Antibody, Alexa Fluor 488 (1:200 dilution)	Invitrogen	Cat#A11034; RRID: AB_2576217
Goat anti-Mouse IgG (H + L) Highly Cross-Adsorbed Secondary Antibody, Alexa Fluor 594 (1:200 dilution)	Invitrogen	Cat#A11032; RRID: AB_2534091

(*Continued on next page*)

Continued

REAGENT or RESOURCE	SOURCE	IDENTIFIER
Goat anti-Rabbit IgG (H + L) Highly Cross-Adsorbed Secondary Antibody, Alexa Fluor 594 (1:200 dilution)	Invitrogen	Cat#A11037; RRID: AB_2534095
Goat Anti-Rabbit IgG Antibody (H + L), Biotinylated	Vector	Cat#BA-1000-1.5
Streptavidin-APC-AlexaFluor 750	Invitrogen	Cat#SA1027
Chemicals, peptides, and recombinant proteins		
BIO	Sigma-Aldrich	Cat#B1686
BrdU	Sigma-Aldrich	Cat#B5002
BSA	Sigma-Aldrich	Cat#A2153
CnT-07 medium	CELLnTEC advanced cell systems	Cat#CnT-07
Cold fish gelatin	Sigma-Aldrich	Cat#G7765
Crystal violet	Sigma-Aldrich	Cat#C0775
DAKO fluorescent mounting medium	DAKO	Cat#S3023
Dispase II	Sigma-Aldrich	Cat#04942078001
DMEM	Gibco	Cat#41965
DMSO	Sigma-Aldrich	Cat#B5002
DNase I	Roche	Cat#10104159001
Formaldehyde	VWR	Cat#9713
Hoechst 33342	Invitrogen	Cat#H3570
Hydrogen peroxidase block	Thermo Fisher Scientific	Cat#TA-125-HP
Lapatinib	Sigma-Aldrich	Cat#SML2259
mIgG	Equitech-Bio	Cat#SLM56
Mitomycin C	Sigma-Aldrich	Cat#M4287
Normal goat serum	Sigma-Aldrich	Cat#G9023
OCT	Sakura	Cat#4583
Paraformaldehyde (PFA)	VWR	Cat#28794
PMSF	Sigma-Aldrich	Cat#P7626
Rhodamine B	Sigma-Aldrich	Cat#R6626
SAG	Sigma-Aldrich	Cat#SML1314
TPCK	Sigma-Aldrich	Cat#T4376
Triton X-100	Fluka	Cat#93418
Critical commercial assays		
ABC Kit	Vector	Cat#PK-4000
DAB	Vector	Cat#SK-4100
LIVE/DEAD Fixable Dead Cell Stain Kit BLUE	Invitrogen	Cat#L23105
Experimental models: Cell lines		
AK23 hybridoma	M. Amagai, gift	Tsunoda et al.[28]
2.4G2 hybridoma	Anne Wilson, gift	Wilson et al.[60]
3T3-J2 mouse fibroblasts, feeder layer cells	H. Green, gift	Rheinwald and Green[84]
Experimental models: Organisms/strains		
B6N.129P2-Axin2^{tm1Wbm}/J (*Axin2*^{LacZ}) mice	Jackson Laboratories	Cat#9120
C57BL/6J mice	Harlan Netherlands	
CD1-Tg(tetO-HIST1H2BJ/GFP)47Efu/J mice	Jackson laboratories	Cat#5104[35]

(*Continued on next page*)

Continued

REAGENT or RESOURCE	SOURCE	IDENTIFIER
Crl:NU(Ico)-*Foxn1*^{nu} (Swiss nude) mice	Charles River	Strain#620
Dsg3+/– mice	M. Röcken, gift	Koch et al.[29]
FVB.Cg-Tg B5Nagy/J (CAG-EGFP) mice	Jackson Laboratories	Cat#3516
FVB/N-Tg(K5-tTA/VP16) mice	A. Glick, gift	Diamond et al.[85]
H2BGFP mice from crossing the following mice: CD1-Tg(tetO-HIST1H2BJ/GFP)47Efu/J mice and FVB/N-Tg(K5-tTA/VP16) mice	From crossing	
Oligonucleotides		
Axin2 Mouse Primer for RT-qPCR	Microsynth	Forward: GGTTCCGGCTATGTCTTTGC Reverse: CAGTGCGTCGCTGGATAACTC
Blimp1 Mouse Primer for RT-qPCR	Microsynth	Forward: GACGGGGGTACTTCTGTTCA Reverse: GGCATTCTTGGGAACTGTGT
Bmp2 Mouse Primer for RT-qPCR	Microsynth	Forward: TGGAAGTGGCCCATTTAGAG Reverse: TGACGCTTTTCTCGTTTGTG
Bmp4 Mouse Primer for RT-qPCR	Microsynth	Forward: CGAGCCAACACTGTGAGGAGT Reverse: AGGTTGAAGAGGAAACGAAAAGC
Cd34 Mouse Primer for RT-qPCR	Microsynth	Forward: CTTCTGCTCCGAGTGCCATT Reverse: CCTGGGCCAACCTCACTTC
Cyclophilin S1 Mouse Primer for RT-qPCR	Microsynth	Forward: GCTGGATGGCAAGCATGTG Reverse: CTGTCTTGGTGCTCTCCACCTT
E-cadherin (Cdh1) Mouse Primer for RT-qPCR	Microsynth	Forward: TGCTGCAGGTCTCCTCATGGCT Reverse: GCCGGCCAGTGCATCCTTCA
Gli1 Mouse Primer for RT-qPCR	Microsynth	Forward: CCCATAGGGTCTCGGGGTCTCAAAC Reverse: GGAGGACCTGCGGCTGACTGTGTAA
Gli2 Mouse Primer for RT-qPCR	Microsynth	Forward: TGAGGAGAGTGTGGAGGCCAGTAGCA Reverse: CCGGGGCTGGACTGACAAAGC
Jup Mouse Primer for RT-qPCR	Microsynth	Forward: CCTGTGGACTCTGCGCAAT Reverse: GACCAGGATCTTCAGCACACTCT
Klf5 Mouse Primer for RT-qPCR	Microsynth	Forward: GGACTCATACGGGCGAGAAGCCCTAC Reverse: GTGCTTCCTGTAGTGGCGGGTCAG
Lgr5 Mouse Primer for RT-qPCR	Microsynth	Forward: CCAATGGAATAAAGACGACGGCAACA Reverse: GGGCCTTCAGGTCTTCCTCAAAGTCA
Lgr6 Mouse Primer for RT-qPCR	Microsynth	Forward: GACCCCCTGACGGCTTACCTAGACCT Reverse: GTGGTTCCCTGAGAGCCGCAG
Lhx2 Mouse Primer for RT-qPCR	Microsynth	Forward: CCTACTACAACGGCGTGGGCACTGT Reverse: GTCACGATCCAGGTGTTCAGCATCG
Lrig1 Mouse Primer for RT-qPCR	Microsynth	Forward: TGACGAATCTGCAGGAAGTG Reverse: TTTCCGTGATGTTGTTGGAA
Nfatc1 Mouse Primer for RT-qPCR	Microsynth	Forward: AACGCCCTGCTGACCACCGATAGCACT Reverse: CCCGGGTGCCTTCCGTCTCATA
Ptch1 Mouse Primer for RT-qPCR	Microsynth	Forward: TGCTGTGCCTGTGGTCATCCTGATT Reverse: CAGAGCGAGCATAGCCCTGTGGTTC
Sca1 Mouse Primer for RT-qPCR	Microsynth	Forward: TGCCCCTACCCTGATGGAGTCTGTG Reverse: GGAGGGCAGATGGGTAAGCAAAGATTG
Shh Mouse Primer for RT-qPCR	Microsynth	Forward: CCCAATTACAACCCCGACAT Reverse: GTCTTTGCACCTCTGAGTCATCA
Sox9 Mouse Primer for RT-qPCR	Microsynth	Forward: CAAGCTCTGGAGGCTGCTGAACGA Reverse: CGGCCTCCGCTTGTCCGTT

(*Continued on next page*)

Continued

REAGENT or RESOURCE	SOURCE	IDENTIFIER
Sufu Mouse Primer for RT-qPCR	Microsynth	Forward: GGAGCCCTCATCCCTCTCTGCCTAA Reverse: TACGGGTGTTCCTCAGTGGCAAAGG
TAp63 Mouse Primer for RT-qPCR	Microsynth	Forward: TGTATCCGCATGCAAGACT Reverse: CTGTGTTGTAGGGGCTGGTGGAC
Tcf4 Mouse Primer for RT-qPCR	Microsynth	Forward: CTACGGAGGGATGCTGGGCAATTCT Reverse: TGGAGTTGATGTCTGCCGAGGAGTG
Tgfβ1 Mouse Primer for RT-qPCR	Microsynth	Forward: CCAAGGAGACGGAATACAGG Reverse: GGTTCATGTCATGGATGGTG
Wnt6 Mouse Primer for RT-qPCR	Microsynth	Forward: TGGAGATATCCGTGCATTGGT Reverse: CGCAGGAACCCGAAAGC
ΔNp63 Mouse Primer for RT-qPCR	Microsynth	Forward: GAAAACAATGCCCAGACTCAA Reverse: TGTGCGTGGGTGTTG
Software and algorithms		
Fiji distribution of ImageJ2 software	https://github.com/fiji	Ver#2.9.0[86]
FlowJo	Treestar	Ver#7.6.1
Image Studio Lite software	LI-COR	Ver#5.2
NIS Elements software	Nikon	Ver#4.40
Openlab software	PerkinElmer	Ver#5.5.2
Prism software	GraphPad	Ver#10.0.0 (153)
ProGres CapturePro software	Jenoptik	Ver#2.7
Other		
BD LSR II Flow cytometer	BD Biosciences	Cat#LSR II
Nikon DS-Qi2 black & white microscope camera	Nikon	Cat#DS-Qi2
Nikon DS-Ri2 color microscope camera	Nikon	Cat#DS-Ri2
Nikon Eclipse Ti	Nikon	Cat#Ti-E
Odyssey Imaging System	LI-COR	Cat#9120
Olympus BX51 microscope	Olympus	Cat#BX51

RESOURCE AVAILABILITY

Lead contact

Further information and requests for resources and reagents should be directed to and will be fulfilled by the lead contact, Eliane J. Müller (eliane.mueller@unibe.ch).

Materials availability

All unique reagents generated in this study are available from the lead contact.

Data and code availability

All data reported in this paper is available within the paper and the supplemental information. This paper does not report original code. The data used to support the findings of this study or any additional information required to reanalyze the data reported will be shared by the lead contact upon request.

EXPERIMENTAL MODEL AND STUDY PARTICIPANT DETAILS

Mice

Study approval

Experiments were approved by the ethics committee, Canton Bern, Switzerland (26/08; BE78.11; BE2_15).

Origins of mice

C57BL/6J (Harlan Netherlands); *Dsg3+/−* mice[29] (kind gift of Martin Röcken, University of Tübingen); CD1-Tg(tetO-HIST1H2BJ/GFP)47Efu/J (Jackson laboratories, stock no. 5104[35]) were crossed with FVB/N-Tg(K5-tTA/VP16) (kind gift of Adam Glick, Pennsylvania State University, Park, and Rune Toftgard, Karolinska Institute, Huddinge[85]) to obtain H2BGFP mice; FVB.Cg-Tg B5Nagy/J (CAG-EGFP, Jackson Laboratories, stock no. 3516); Crl:NU(Ico)-*Foxn1*^{nu} (Swiss nude mice, Charles River); B6N.129P2-Axin2^{tm1Wbm}/J (*Axin2*^{LacZ} mice, Jackson Laboratories, stock no. 9120).

Cells

Primary keratinocytes from C57BL/6J, *Dsg3* wildtype or *Dsg3−/−* mouse embryos were isolated as we reported previously.[87]

METHOD DETAILS

Mice treatments

Dsg3−/− and *Dsg3+/−* were obtained through breeding of *Dsg3+/−* mice and entered experiments at postnatal day15 (P15, day −3 before onset of telogen). Two and a half- (1st telogen, P20, day 0) or 8- (2nd telogen, P56, day 0) week-old, sex-matched C57BL/6J and eight-week-old tetOFF H2BGFP,[35] CAG-EGFP and Axin2-LacZ mice were s.c. injected once at the back with 12.5μg/g (body weight) of AK23[28] or control mIgG (Equitech-Bio),[27] except if mentioned otherwise. In general, all mice received softened pellets mixed with honey as well as protein supplements in the drinking water to minimize oral lesions. Under this regimen, daily monitored weight loss was less than 10%, and no spontaneous hair loss or skin erosions until the end of the experiment when mice were sacrificed. However, weakened hair shaft anchorage assessed by tape striping after euthanasia was apparent in AK23-injected mice (telogen 1 and 2), as reported previously,[27] as well as in *Dsg3−/−* mice (telogen 1). Tape stripping was done manually and must be considered semi-quantitative. Strips with attached hairs were scanned and converted into black and white signals, representing tape coverage, which was quantified using Fiji.[86] Blistered HFBus were counted on H&E sections under a light microscope (>50 HFBus per animal). Simultaneous, histopathological inspection showed no difference in the density, distribution or composition of dermal infiltrates between control, treated or knockout mice, nor was a peri-follicular inflammation present. These findings were confirmed by a board-certified dermatopathologist (Laurence Feldmeyer) for AK23 and mIgG injected mice (from day 1 to day 6; n = 1 per time point). They are in line with consistent blistering in AK23-injected *Rag2−/−* mice (no mature T or B lymphocytes)[27] and early reports on lack of an essential contribution of supplement or the Fc-portion of PV IgG (including Dsg3 clustering) to the blistering phenotype of antibody-treated neonatal mice or cultured mouse keratinocytes.[88,89]

Before antibody injection, the following pre-treatments were performed; for label retention studies, 4-week-old tetOFF H2BGFP mice received 0.2 g/kg Doxycycline chow (Provimi Kliba) for 4 weeks; for Lapatinib, BIO or SAG treatment, 8-week-old female C57BL/6J mice were subcutaneously injected at the back after titration (Figure S4) with 9μg/g Lapatinib (Sigma-Aldrich), 10μg/g BIO (Sigma-Aldrich) or 5μg/g SAG (Sigma-Aldrich) in 130μL DMSO (30%) diluted in PBS 4h prior to mIgG/AK23 administration or 4 and 5 days after AK23 administration. Drug concentrations were defined by dose response by means of blistered HFBus (Figure S4A). Control animals were s.c. injected at the back with 130μL DMSO (30%) diluted in PBS without drugs; for BrdU incorporation, 8-week-old C57BL/6J mice were intraperitoneally injected with 50μg/g (BW) BrdU (Sigma-Aldrich, 5-Bromo-2′-Deoxyuridine) 1day prior to euthanasia.

Protein extraction, immunoblotting and RT-qPCR

For protein and RNA analyses, mouse back skin of euthanized mice was excised and directly processed as described previously.[27] Specifically, immunoblotting of Triton X-100 soluble fractions, protein levels were normalized to beta-Tubulin (Abcam) and for Triton X-100 insoluble fractions to Lamin B1 (Abcam). Quantification of antibody signals was done using the double-laser Odyssey device (Licor).

Antibodies for immunoblotting and primers for RT-qPCR are provided in key resources table.

Immunolabeling of mouse back skin biopsy sections and cell cultures

Prior to OCT embedding, back skin biopsies were incubated at 4°C for 3h in 15% sucrose, followed by an overnight incubation at 4°C in 30% sucrose, embedded in OCT (TissueTek, Sakura) on liquid nitrogen and stored at −80°C. 8μm frozen sections were fixed in 4% PFA for 10 min at RT, washed in PBS^{+} (PBS with 0.9 mM calcium and 0.98 mM magnesium) for 3 × 5min before blocking. Prior to paraffin embedding, back skin biopsies were fixed in 4% formaldehyde overnight, processed for paraffin embedding, sectioned and de-paraffinized according to standard protocols. Antigen retrieval was done by heating slides in TE buffer pH8.0 for 3 × 5min in a microwave. Sections were allowed to cool down at 4°C for 20min, washed in PBS^{+} for 3 × 5min before blocking. All sections were blocked with 10% normal goat serum (Sigma-Aldrich), 1% BSA (Sigma-Aldrich), 0.1% Triton X-100 (Fluka), 2% cold fish gelatin (Sigma-Aldrich) in PBS^{+} in a humid chamber for 1h at RT. For immunofluorescence analyses, antibodies were diluted in blocking buffer and incubated overnight at 4°C in a humid chamber. OCT embedded sections were washed in 0.5M EDTA pH8.0, 1M $MgCl_2$, 10% Triton X-100 in PBS^{+} for 3 × 5min, paraffin embedded sections were washed in PBS^{+} for 3 × 5min. Secondary antibodies (Alexa Fluor 488, 594, 1:200, Invitrogen) were diluted in blocking buffer and were incubated in a humid chamber for 1.5 h at RT. Nuclei were counterstained with Hoechst 33342 (1:3000, 1 mg/ml, Invitrogen) and sections were washed in PBS^{+} for 3 × 5min before mounting.

For the detection of BrdU, OCT sections were fixed with 4% PFA for 20 min at RT. Nuclei were permeabilized with 0.5% Triton X-100, 2mM PMSF (Sigma-Aldrich), 2mM TPCK (Sigma-Aldrich) in PBS^{+} for 10 min at RT. After washing with PBS^{+}, sections were treated with 7.5U/mL

DNase I (Roche) in PBS$^+$ at 37°C for 30 min. Subsequent immunolabeling was performed as described above. For immunohistochemical detection of p-β-catenin or GFP, a hydrogen peroxidase block (Thermo Fisher Scientific) was applied for 10 min at RT and slides were washed 3 × 5min PBS$^+$. Blocking and primary antibody incubation was performed as described above. Sections were washed 3 × 5min with 0.2% Triton X-100 in PBS$^+$ at 50°C–60°C, incubated with a biotinylated anti-rabbit antibody (Vector) at 1:200 for 30 min at RT, rinsed and incubated with the ABC Kit (Vector) for 20 min at RT. After a final washing, DAB (Vector) was developed for 5min and slides were counterstained with Hematoxylin (Baxter). All slides were mounted with DAKO fluorescent mounting medium (DAKO) and kept at 4°C for at least 6h prior to analysis. For direct immunofluorescence labeling of cultured cells, confluent C57BL/6J, *Dsg3* wildtype or *Dsg3*−/− keratinocytes were exposed to elevated calcium (1.2mM) in CnT-07 medium (CELLnTEC advanced cell systems) for 24h. Cells were then incubated on ice with AK23 or mIgG in 1% BSA in PBS+ (PBS with 0.9mM calcium and 0.98mM magnesium; 20μg/ml) for 2hrs. Cells were washed and fixed with 1% paraformaldehyde in PBS+ for 20 min at room temperature, and thoroughly washed before incubation with secondary antibody in 1% BSA-PBS+ for 1h at room temperature. Nuclei were stained using Hoechst 33342 (1 mg/mL, 1:1500) and samples pictured with a Nikon Eclipse Ti immunofluorescence microscope. Images were processed either with Openlab 5.5.2 software (PerkinElmer) or NIS Elements 4.40 software (Nikon). For immunohistochemistry, analysis was done with an Olympus BX51 microscope and images were processed using ProGres CapturePro 2.7 (Jenoptik).

Colony forming efficiency assay

Keratinocytes were isolated from back skin of 8-week-old mice treated with AK23 or mIgG for the indicated time points as per Jensen and colleagues,[90] except that DMEM and FAD were replaced with chemically defined medium CnT-07 (CELLnTEC advanced cell systems). 280 keratinocytes/cm^2 isolated from adult mouse skin were plated onto 10μg/mL Mitomycin C (Sigma-Aldrich) treated J2 3T3 feeder layers (a kind gift of Howard Green, Harvard Medical School, Boston[84]) for 2 h and cultured for 14 days. Colonies were fixed overnight with 4% PFA and stained with 1% Rhodamine B (Sigma-Aldrich). Cells from a minimum of three mice per treatment group were isolated and plated in triplicates. Growing (holoclone-like) and non-growing (non holoclone-like) colonies were evaluated as described by Barrandon et al.,[91] and counted under a stereo-microscope. Actively growing colonies were confirmed by immunolabeling after cells were cultured on 10μg/mL Mitomycin C treated J2 3T3 feeder cells in 2-well *Lab-Tek* chamber slides (Thermo Fisher Scientific) for 14 days (Figure S2C). Three hours prior to fixation BrdU (Sigma-Aldrich) was added to culture medium and allowed to incorporate into dividing cells. For BrdU detection and immunolabeling, colonies were fixed with 4% PFA for 10 min at RT, permeabilized with 0.5% Triton X-100, 2mM PMSF (Sigma-Aldrich), 2mM TPCK (Sigma-Aldrich) in PBS$^+$ (containing 0.2mM $CaCl_2$) for 10 min at RT and treated with 7.5U/mL DNase I (Roche) in PBS$^+$ at 37°C for 30 min. Sections were stained with primary antibodies diluted in 1% BSA-PBS$^+$ overnight at 4°C, and incubated with secondary antibodies (Alexa Fluor 488, 594, 1:500, Invitrogen) for 1h at RT. Washings were done using PBS$^+$. Nuclei were counterstained with Hoechst 33342 (1:3000, 1 mg/mL, Invitrogen).

Flow cytometry

Keratinocytes were isolated from skin which was cut into pieces and incubated in Trypsin-EDTA/PBS (0.2%/0.08%) (Amimed) for 2h at 32°C. The epidermis was gently scraped off and incubated for 20min in DMEM/10% FCS on a magnetic stirrer to dissociate the cell sheet. The cell suspension was filtered through a 70μm and 40μm mesh filter (BD), washed and counted. Cell suspensions were then incubated on ice for 45min with a mix of primary antibodies in CnT-02/1% BSA and diluted 1:1 with the supernatant of 2.4G2 hybridoma (kind gift of Anne Wilson, LICR, Lausanne) producing a CD16/CD32 antibody to block unspecific binding. Primary antibodies used are listed in key resources table. Isotype controls were as indicated on the datasheets of primary antibodies. Primary keratinocytes from mice without BrdU injection served as negative control. After washing in CnT-02/1% BSA, cells were incubated with Streptavidin-APC-AlexaFluor 750 (Invitrogen) for 20min on ice, washed in PBS, and to exclude dead cells, stained with LIVE/DEAD Fixable Dead Cell Stain Kit BLUE (Invitrogen) according to the manufacturer's protocol. After gating for keratinocytes using FSC/SSC, LIVE/DEAD-/CD31-/CD45, a minimum of 50'000 cells were acquired on an LSRII flow cytometer (BD). Subsequent analyses were done using FlowJo 7.6.1 (Treestar Inc.).

Hair plucking

Eight-week-old C57BL/6J mice, injected with mIgG/AK23 2days before plucking, were shortly immobilized by Isoflurane inhalation and hairs were plucked with wax strips on a 5 × 3 cm area on the back. Mice were euthanized at day6 or 9 after hair plucking. Anagen hair eruption was observed macroscopically, and biopsies taken from the plucked area were sectioned and stained for H&E to evaluate the hair cycle stage.

Quantification of LacZ expression

Back skin biopsies (max. width 2mm, max. thickness 2mm) from mIgG/AK23 injected Axin2-LacZ mice were pre-fixed in 2% PFA/0.2% glutaraldehyde in PBS for 1h at 4°C, washed 3 × 20min in PBS and X-Gal staining (10 mg/mL X-Gal containing 5mM K-Ferrocyanide, 5mM K-Ferricyanide and 2mM $MgCl_2$ in PBS) performed at 22°C for 24h.[92] After 3 × 20min washing in PBS$^+$, biopsies were fixed in 4% PFA at 4°C overnight. Biopsies were embedded in paraffin. LacZ quantification above background was done with the Fiji software using the red channel.

Reconstitution assay for multipotency

"Pocket grafting" of primary keratinocytes was performed as described by Claudinot et al.[39] Donor cells (5x 10^5) isolated from mIgG/AK23 injected CAG-EGFP mice, were diluted in DMEM/10% BSA and injected into the dermal-epidermal junction of P0-C57BL/6J mouse skin. The pocket was created by incubating back skin slices in 2% EDTA, pH 7.4 at 37°C for 2.5h and separation of the IFE from the dermis with a micro syringe (BD Micro-Fine 0.3 mL). Cells were allowed to adhere, and pockets were transplanted onto the back of adult Swiss nude mice, sutured and covered with a nude mouse skin flap for protection. The flap was removed at day14 after surgery. Grafting was performed in quadruplicates of pooled cells per treatment group. On day25 nude mice were pictured and euthanized at day77 and skin reconstitution of mIgG and AK23 treated keratinocytes assessed by immunolabeling for GFP.

Keratinocyte dissociation assay

Primary keratinocytes from C57BL/6J, *Dsg3* wildtype or *Dsg3*−/− mouse embryos were isolated as we reported previously,[87] and intercellular adhesive strength tested by our established keratinocyte dissociation assay.[89,93] Keratinocytes (40,000 cells/cm^2) were seeded into 24 well plates (TPP Techno Plastic Products AG). At 100% confluency, calcium in the medium was increased to 1.2mM for 24hrs and keratinocytes treated with either no antibody or 20μg/mL AK23 or 20μg/mL mIgG for 24hrs. The cell monolayer was then detached using 400μL of 4.8 U/mL dispase II (Sigma Aldrich) for 20 min at 37°C, 95% humidity and 5% CO_2 and the floating cell sheets subjected to mechanical stress (250μL volume pipetted once using a 1mL Gilson pipette with pipette tips coated with 0.1% BSA). The resulting fragments were fixed with 400μL 4% formaldehyde (VWR), stained with 4.5μL 0.1% crystal violet (Sigma Aldrich), and counted.

QUANTIFICATION AND STATISTICAL ANALYSIS

Quantification of LacZ expression

Back skin biopsies (max. width 2mm, max. thickness 2mm) from mIgG/AK23 injected Axin2-LacZ mice were pre-fixed in 2% PFA/0.2% glutaraldehyde in PBS for 1h at 4°C, washed 3 × 20min in PBS and X-Gal staining (10 mg/mL X-Gal containing 5mM K-Ferrocyanide, 5mM K-Ferricyanide and 2mM MgCl2 in PBS) performed at 22°C for 24h.87 After 3 × 20min washing in PBS+, biopsies were fixed in 4% PFA at 4°C overnight. Biopsies were embedded in paraffin. LacZ quantification above background was done with the Fiji software using the red channel.

Fragments count keratinocyte dissociation assay

Cell sheet fragments were fixed with 400μL 4% formaldehyde (VWR), stained with 4.5μL 0.1% crystal violet (Sigma-Aldrich), and imaged using 1 J5 camera (Nikon, Japan). Counting was performed using the automated counting feature by Fiji software, fragments smaller than 0.0125cm^2 were excluded.

Statistical analysis

Results are shown as mean ± SEM. All tests applied were non-parametric as defined by the Anderson-Darling p-value test ($p < 0.05$). Data, except for the keratinocyte dissociation assay, were analyzed by a 2-tailed Student's *t* test using GraphPad Prism software. For the dissociation assay, two-way ANOVA with Tukey post-hoc test was used. Asterisks denote statistical significance (*$p < 0.05$; **$p < 0.01$; and ***$p < 0.001$).